Aparicio, S.; Serna-García, R.; Seco, A.; Ferrer, J.; Borrás Falomir, L.; Robles, Á. (2022). Global sensitivity and uncertainty analysis of a microalgae model for wastewater treatment. Science of The Total Environment. 806(1):1-15. https://doi.org/10.1016/j.scitotenv.2021.150504

Global sensitivity and uncertainty analysis of a microalgae model for wastewater treatment.

Stéphanie Aparicio[a]*, Rebecca Serna García[a], Aurora Seco[a], José Ferrer[b], Luis Borrás Falomir[a], Ángel Robles[a]

[a]CALAGUA – Unidad Mixta UV-UPV, Departament d'Enginyeria Química, Universitat de València, Avinguda de la Universitat s/n, 46100, Burjassot, València, Spain

[b]CALAGUA – Unidad Mixta UV-UPV, Institut Universitari d'Investigació d'Enginyeria de l'Aigua i Medi Ambient – IIAMA, Universitat Politècnica de València, Camí de Vera s/n, 46022, València, Spain.

*Corresponding author

Email address: stephanie.aparicio@uv.es (Stéphanie Aparicio Antón)

ABSTRACT

The results of a global sensitivity and uncertainty analysis of a microalgae model applied to a Membrane Photobioreactor (MPBR) pilot plant were assessed. The main goals of this study were: (I) to identify the sensitivity factors of the model through the Morris screening method, i.e. the most influential factors; (II) to calibrate the influential factors online or offline; and (III) to assess the model's uncertainty. Four experimental periods were evaluated, which encompassed a wide range of environmental and operational conditions. Eleven influential factors (e.g. maximum specific growth rate, light intensity and maximum temperature) were identified in the model from a set of 34 kinetic parameters (input factors). These influential factors were preferably calibrated offline and alternatively online. Offline/online calibration provided a unique set of model factor values that were used to match the model results with experimental data for the four experimental periods. A dynamic optimization of these influential factors was conducted, resulting in an enhanced set of values for each period. Model uncertainty was assessed using the uncertainty bands and three uncertainty indices: p-factor, r-factor and ARIL. Uncertainty was dependent on both the number of influential factors identified in each period and the model output analyzed (i.e. biomass, ammonium and phosphate concentration). The uncertainty results revealed a need to apply offline calibration methods to improve model performance.

Keywords: Dynamic optimization; Microalgae model; MPBR; Municipal wastewater; Sensitivity analysis; Uncertainty analysis.

HIGHLIGHTS

- A global sensitivity and uncertainty analysis of a microalgae model was conducted.
- Eleven factors out of 34 were identified as influential and were calibrated offline/online.
- Four different experimental periods were properly represented by a single set of model factors.
- The uncertainty bandwidth revealed a need to apply offline calibration procedures.

1. Introduction

Microalgae-based wastewater treatment represents a promising biological system to treat different wastewater sources in a way that can transform conventional wastewater treatment plants (WWTPs) into water resource recovery facilities (WRRFs) (Seco et al., 2018). Photoautotrophic microalgae use light energy, inorganic carbon and nutrients (inorganic nitrogen and phosphorus) for growth. Solar energy and nutrients are harvested in form of microalgae biomass while inorganic carbon is biofixed. Microalgae-based wastewater treatment can reduce treatment costs, generate clean water and reduce the environmental impact of the process (Seco et al., 2018).

An in-depth knowledge of the processes involved in microalgae metabolism is required to better understand how to operate microalgae-based technologies, how to optimize processes associated, how to improve reactor design and how to select the best control strategies to enhance pollutant removal efficiency. Microalgae and traditional activated sludge systems are intrinsically complex, since both depend on environmental variables such as temperature, pH, substrate availability, etc. However, it should be noted that photoautotrophic microalgae metabolism is not only affected by the environmental factors that influence activated sludge but also by seasonal and daily fluctuations in light intensity (González-Camejo et al., 2018). The correct operation of microalgae-based wastewater treatments thus demands a robust, feasible and efficient tool to forecast the culture development and its compliance with increasingly stringent regulations. Mathematical models can help to study the main processes and variables that influence algal metabolism in different culture media, including municipal wastewater.

An array of mathematical models for predicting microalgae growth has been developed in the last ten years (Costache et al., 2013; Eze et al., 2018; Ndiaye et al., 2018; Ruiz et al., 2013; Solimeno et al., 2015, 2017; Wágner et al., 2016). This process cannot be considered a well-characterized system, since some model

54 factors are uncertain and speciation-dependent. The ammonium semi-saturation constant has been
55 reported to range from 0.1 to 31.5 g N m-3 (Aslan and Kapdan, 2006; Solimeno et al., 2017), and is a perfect
56 example of the intrinsic variability and uncertainty of model factors, so that the application of these models
57 requires a great number of assumptions regarding the simplification of biological processes and model
58 factors. These assumptions are sources of uncertainty that could propagate through the model thus
59 generating uncertainty in the model outputs. The resulting uncertainty in the model results could lead to
60 misleading decisions during process design and/or optimization. Hence, performing a global sensitivity and
61 uncertainty analysis (GSA and UA, respectively) would help to deal with these issues by analysing and
62 understanding model performance. GSA involves identifying the most important model factors to be
63 calibrated, while UA entails determining the model output uncertainty derived from uncertain model input
64 factors (Rajabi et al., 2020). GSA and UA should be performed concurrently, as both are essential parts of
65 the model development process in design optimization, reliability analysis, and data-worth analysis (Rajabi
66 et al., 2020). To the best of the authors' knowledge, both GSA and UA have not been performed concurrently
67 in mathematical models for wastewater treatment with microalgae. Therefore, no information is available on
68 the microalgae models' most influential factors and the variability of the uncertainty of model output.

69 Although, the mechanistic microalgae model proposed by Viruela et al. (2021) was validated using 4
70 experimental periods, which combine key environmental and operational conditions characteristic of a
71 microalgae-based wastewater treatment, the uncertainty of model parameters could lead to uncertainty
72 propagations on modelling results, reducing its practical application. Thus, this study tends to address data
73 gaps related to uncertainty on microalgae-based wastewater treatment models, based on Viruela et al.
74 (2021), by performing a GSA and UA. The Morris screening method was applied as GSA method to identify
75 the most influential factors of the model, which were calibrated through offline (obtained from experimental
76 assays) and online (variation of model parameters to match model predictions to experimental results)
77 methodologies. For further enhancing the model performance, the calibrated values for the influential factors
78 were dynamically optimized using online data. Model uncertainty was analyzed and quantified from Monte
79 Carlo simulations and three uncertainty coefficients: the p-factor, the r-factor and the Average Relative

Interval Length (ARIL). A calibration protocol was also recommended to reduce model uncertainty by means of prioritizing different calibration methodologies.

Hence, this work could be seen as the first study to simultaneously perform GSA and UA in the field of microalgae-based wastewater treatment modelling, while proposing a set of input factors to be calibrated by a given protocol.

2. Material and methods

2.1. The mathematical model

The model used in this work (Viruela et al., 2021) simulated microalgae growth from different phosphorus and nitrogen sources. Regarding phosphorus source, the microalgae had two different metabolic pathways: under phosphorus-replete conditions, microalgae uptake dissolved extracellular phosphate (S_{PO4}) to support their vital metabolic functions and stored part of the excess in form of intracellular polyphosphate ($X_{PP\text{-}ALG}$) while under phosphorus-starved conditions they consumed their $X_{PP\text{-}ALG}$ reservoirs to grow. In terms of nitrogen source, microalgae can use ammonium-ammonia (S_{NHX}, both are considered in chemical equilibrium) and nitrate (S_{NO3}), although different authors state that microalgae prefer S_{NHX} over S_{NO3} when both are present simultaneously (Kim et al., 2013; Markou et al., 2014; Nagase et al., 2001; Pastore et al., 2020). To represent the microalgae's preference for the nitrogen-reduced form, an inhibition switching function of S_{NHX} was included for microalgae growth on S_{NO3}. González-Camejo et al. (2019) and Shoener et al. (2019) reported that S_{NO3} uptake rate was lower than S_{NHX}, so that nitrate related growth kinetic expressions have a specific growth rate reduction factor. Microalgae growth was modeled as a biomass of non-specific photosynthetic organisms (X_{ALG}) by combining Monod-type kinetics for five components: S_{PO4}, $X_{PP\text{-}ALG}$, S_{NHX}, S_{NO3}, and inorganic carbon source ($S_{Ig,C}$) (Table 1). The storage of $X_{PP\text{-}ALG}$ was modeled through the Hill equation and Monod kinetics for S_{PO4}, potassium (S_K) and magnesium (S_{Mg}), since $X_{PP\text{-}ALG}$ composition was assumed as $(K_{0.34}Mg_{0.33}PO_3)_n$. The five processes described above are influenced by three environmental factors: light, pH and temperature factor (described below in Section 2.4.1). The endogenous respiration and decay processes of the particulate components (X_{ALG} and $X_{PP\text{-}ALG}$) were also considered in the model. These were light intensity and pH-independent, being affected only by thermal variations. As the storage product of $X_{PP\text{-}ALG}$ was considered separately from X_{ALG}, this component was subjected to a separate

decay process. The model included the stripping processes for free ammonia ($S_{[NH3]}$), oxygen (S_{O2}) and carbon dioxide ($S_{[CO2]}$). The processes described above together gave rise to a model comprising a total of 11 different processes: X_{ALG} growth on S_{NHX} and S_{PO4}, X_{ALG} growth on S_{NO3} and S_{PO4}, X_{ALG} growth on S_{NHX} and X_{PP-ALG}, X_{ALG} growth on S_{NO3} on X_{PP-ALG}, X_{PP-ALG} storage, X_{ALG} endogenous respiration, X_{ALG} lysis, X_{PP-ALG} lysis, $S_{[CO2]}$ stripping, S_{O2} stripping and $S_{[NH3]}$ stripping. The model process kinetics are summarized in Table 1.

The 13 components considered for the model were classified as soluble (described with S-index) and particulate (described with X-index): soluble oxygen S_{O2}, soluble ammonia-ammonium nitrogen S_{NHX}, soluble nitrate nitrogen S_{NO3}, soluble phosphate S_{PO4}, soluble inorganic carbon $S_{Ig,C,}$ proton S_H, soluble magnesium S_{Mg}, soluble potassium S_K, readily biodegradable soluble organic matter S_S, inert soluble organic matter S_I, microalgae biomass X_{ALG}, inert particulate organic matter X_I and polyphosphates stored by microalgae X_{PP-ALG}.

Microalgae biomass (X_{ALG}) was quantified as volatile suspended solids (VSS). In order to compare experimental and simulated results, two additional components were included: total suspended solids (X_{TSS}, g TSS m^{-3}) and volatile suspended solids (X_{VSS}, g VSS m^{-3}). X_{TSS} was considered as the sum of X_{ALG}, X_I, and X_{PP-ALG} while X_{VSS} was the sum of X_{ALG} and X_I. The modeled and experimental data were thus compared through X_{VSS}. For stoichiometry matrix, conversion factors and further details of the microalgae model the reader is referred to the literature (Viruela et al., 2021).

Table 1. Processes kinetics included in microalgae model developed by Viruela et al. (2021).

Processes j	Processes rate [M L^{-3} T^{-1}]
1. X_{ALG} growth on S_{NHX} and S_{PO4}	$\mu_{ALG} \cdot \frac{S_{Ig,C}}{K_{Ig,C}+S_{Ig,C}} \cdot \frac{S_{NHX}}{K_{NHX}+S_{NHX}} \cdot \frac{S_{PO4}}{K_{PO4}+S_{PO4}} \cdot X_{ALG} \cdot f_L \cdot f_{pH} \cdot f_T$
2. X_{ALG} growth on S_{NO3} and S_{PO4}	$\mu_{ALG} \cdot \eta_{NO3} \cdot \frac{S_{Ig,C}}{K_{Ig,C}+S_{Ig,C}} \cdot \frac{K_{NHX}}{K_{NHX}+S_{NHX}} \cdot \frac{S_{PO4}}{K_{PO4}+S_{PO4}} \cdot \frac{S_{NO3}}{K_{NO3}+S_{NO3}} \cdot X_{ALG} \cdot f_L \cdot f_{pH} \cdot f_T$
3. X_{ALG} growth on S_{NHX} and X_{PP-ALG}	$\mu_{ALG} \cdot \frac{S_{Ig,C}}{K_{Ig,C}+S_{Ig,C}} \cdot \frac{S_{NHX}}{K_{NHX}+S_{NHX}} \cdot \frac{K_{I,PO4}}{K_{I,PO4}+S_{PO4}} \cdot \frac{\frac{X_{PP-ALG}}{X_{ALG}}}{K_{XPP-ALG}+\frac{X_{PP-ALG}}{X_{ALG}}} \cdot X_{ALG} \cdot f_L \cdot f_{pH} \cdot f_T$
4. X_{ALG} growth on S_{NO3} on X_{PP-ALG}	$\mu_{ALG} \cdot \eta_{NO3} \cdot \frac{S_{Ig,C}}{K_{Ig,C}+S_{Ig,C}} \cdot \frac{K_{NHX}}{K_{NHX}+S_{NHX}} \cdot \frac{K_{I,PO4}}{K_{I,PO4}+S_{PO4}} \cdot \frac{S_{NO3}}{K_{NO3}+S_{NO3}} \cdot \frac{\frac{X_{PP-ALG}}{X_{ALG}}}{K_{XPP-ALG}+\frac{X_{PP-ALG}}{X_{ALG}}} \cdot X_{ALG} \cdot f_L \cdot f_{pH} \cdot f_T$
5. X_{PP-ALG} storage	$q_{PP-ALG} \cdot \frac{S_{PO4}}{K_{PO4}+S_{PO4}} \cdot \frac{S_{Mg}}{K_{Mg}+S_{Mg}} \cdot \frac{S_K}{K_K+S_K} \cdot \frac{{K_{XPP-qXPP}}^n}{{K_{XPP-qXPP}}^n+\left(\frac{X_{PP-ALG}}{X_{ALG}}\right)^n} \cdot X_{ALG} \cdot f_L \cdot f_{pH} \cdot f_T$
6. X_{ALG} endogenous respiration	$b_{ALG,1} \cdot X_{ALG} \cdot f_T$
7. X_{ALG} lysis	$b_{ALG,2} \cdot X_{ALG} \cdot f_T$
8. X_{PP-ALG} lysis	$b_{ALG,2} \cdot X_{PP-ALG} \cdot f_T$
9. $S_{[CO2]}$ stripping	$K_{La,CO2} \cdot \left(S_{[CO2]} - S^*_{[CO2]}\right)$
10. S_{O2} stripping	$K_{La,O2} \cdot (S_{O2} - S^*_{O2})$
11. $S_{[NH3]}$ stripping	$K_{La,NH3} \cdot \left(S_{[NH3]} - S^*_{[NH3]}\right)$

2.2. Case studies

The outdoor MPBR pilot plant under study was located in the "Cuenca del Carraixet" WWTP (39°30'04.0''N 0°20'00.1''W, Valencia, Spain). The MPBR pilot plant was fed with effluent from an anaerobic membrane bioreactor (AnMBR) system on the same premises. The MPBR consisted of two 0.25-m and two 0.10-m wide flat panel photobioreactors (PBRs), all with a surface area of 2.3 m^2 (1.15 x 2 m; H x L), and a 14-L working volume membrane tank (MT) equipped with one commercial ultrafiltration hollow-fiber membrane system (PURON® Koch Membrane Systems (PUR-PSH31), 0.03 µm pore) with a filtration area of 3.4 m^2. The PBRs were air-stirred to promote complete mixing of culture medium. Stirring the PBR also promotes carbon stripping as carbon dioxide. Pure CO_2 was injected into the stirring system to set pH to 7.5, ensuring not only an inorganic carbon-rich culture, but also to reduce uncontrolled phosphorus precipitation and ammonia stripping. The temperature of the biomass culture was controlled by a cooling device and thermostat (Daikin R410A inverter). Besides natural light, twelve LED lamps (Unique Led IP65 WS-TP4S-40W-ME) placed at the back of the PBRs continuously illuminated the microalgae culture at a constant irradiance of 300 µmol m^{-2} s^{-1}. Allylthiourea (ATU) was added to keep a constant concentration of 5 mg L^{-1} to inhibit nitrifying bacteria. For further details of the MPBR pilot plant see González-Camejo et al. (2020).

Real-time information on the process operation and conditions was obtained from a control network consisting of pH sensors (pHD sc DPD1R1, Hach Lange), dissolved oxygen-temperature sensors (LDO Hach Lange) and light irradiance sensors (Apogee Quantum SQ-200) to measure only photosynthetically active radiation (PAR). Data acquisition from the online sensors was previously described in Viruela et al. (2018).

Four operation periods were selected from the MPBR pilot plant performance. This analysis is divided into these 4 periods, which are the guiding threads to perform GSA and UA. The 4 periods represent the key variations observed during the three years of the MPBR pilot plant operation, i.e. daily variations in light intensity and temperature, phosphorus-replete and phosphorus-starved conditions in the culture medium, and different operational conditions. Datasets related to the periods selected are shown in Table 2. There were remarkable changes in the daily PAR averages in Periods 1 and 2, reaching minimum values of 10 and 67 µmol m^{-2} s^{-1} and maximum values of 406 and 394 µmol m^{-2} s^{-1} for Period 1 and Period 2, respectively. The difference between the PBR widths and VSS concentration in Period 1 (0.10-m reactor width and VSS

of 1063 ± 141 g VSS m^{-3}) and Period 2 (0.25-m reactor width and VSS of 445 g VSS m^{-3}) revealed significant information on the model sensitivity and uncertainty towards the light intensity constants. Period 3 was mainly characterized by negligible S_{PO4} concentrations (phosphorus-starved conditions). As the model approach stipulates that microalgae should grow in this period by consuming the stored X_{PP-ALG}, the model factors related to X_{PP-ALG} consumption could have influenced the simulation results. Although PBR temperature was controlled, thermal fluctuations of up to 8°C in culture medium were recorded during warm periods, as in experimental Period 4. Bearing in mind that all kinetic expressions of biological processes are regulated by a thermal factor (explained and developed in Section 2.4.1), the model should have been sensitive to cardinal temperatures.

Table 2. Environmental and operational conditions for the 4 selected experimental periods. VSS: volatile suspended solids in PBRs; PO_4-P soluble phosphate in PBRs; PAR: photosynthetically active radiation recorded on PBR surface area; T: culture temperature; and pH: culture pH. The MIN, MAX and AVG sub-indexes refer to the minimum, maximum and average values respectively.

		Period 1	Period 2	Period 3	Period 4
PBR width	m	0.10	0.25	0.10	0.25
VSS	g VSS m^{-3}	1063 ± 141	445 ± 80	830 ± 136	252 ± 36
NH_4-N	g N m^{-3}	16 ± 6	34 ± 4	11 ± 7	42 ± 6
PO_4-P	g P m^{-3}	3.7 ± 0.9	3.2 ± 0.9	0.14 ± 0.11	4.74 ± 1.12
PAR_{MIN}	µmol m^{-2} s^{-1}	10	67	284	112
PAR_{MAX}	µmol m^{-2} s^{-1}	406	394	394	290
PAR_{AVG}	µmol m^{-2} s^{-1}	214 ± 133	258 ± 114	345 ± 36	259 ± 50
T_{MIN}	ºC	20	24.82	23.2	24
T_{MAX}	ºC	26	28.18	24.30	32
T_{AVG}	ºC	24 ± 2	26.14 ± 1.03	23.8 ± 0.4	27 ± 2
pH_{MIN}	-	7.32	7.00	7.08	7.36
pH_{MAX}	-	7.55	7.40	7.37	7.68
pH_{AVG}	-	7.40 ± 0.06	7.2 ± 0.2	7.18 ± 0.08	7.50 ± 0.08

The following parameters were monitored (APHA, 2005) in the influent, the algae culture medium and the permeate: total suspended solids (TSS) 2540-TSS-D, VSS 2540-VSS-E, soluble chemical oxygen demand (sCOD) 5220-COD-D, ammonium nitrogen (NH_4-N), nitrate nitrogen (NO_3-N) 4500-NO3-H, and phosphate (PO_4-P) 4500-P-F). The optical density at 680nm (OD_{680}) was measured with a portable fluorometer

AquaPen-C AP-C 100 (Photon Systems Instruments). For more specific details on the analytical procedures see Viruela et al. (2021).

2.3. Sensitivity analysis

GSA was performed through the Morris screening method (Morris, 1991) to identify the model's most influential factors, reducing the size of parameter set to be calibrated. The Morris screening method was selected from other classical methodologies (e.g. Standardized Regression Coefficients, Sobol indices, or Fourier amplitude sensitivity testing) since it is widely used for GSA in the field of wastewater treatment (see e.g. Corominas and Neumann, 2014; Robles et al., 2014a, Robles et al., 2014b; Ruano et al., 2011; Sin et al., 2011; Solimeno et al., 2016; Sun et al., 2015), it represents a well-stablished methodology for data processing, and it is characterized by a relative simple interpretation.

The Morris screening method is a one-factor-at-a-time (OAT) GSA method that evaluates the distribution of the elementary effects (EE_i) of each input factor upon model outputs, used to calculate the statistical parameters that provide sensitivity results. The scaled elementary effect (SEE_i) proposed by Sin and Gernaey (2009) was applied. The finite distribution of SEE_i associated with each input factor (i.e. F_i) is usually obtained by sampling different coordinates (X) from the parameter space at random. However, this random sampling of X could only cover a reduced part of the space. Campolongo et al. (2007) proposed a modification of the Morris screening method by improving the sampling strategy. In this study, the trajectory-based sampling strategy proposed in Ruano et al. (2012) was applied. From the generated matrices, it determines the distribution of SEE_i of each input factor on the model output. Finally, the distribution of SEE_i is analyzed to determine the relative importance of the input factors and obtain a good approximation of a GSA. Specifically, the selected statistical parameters to evaluate these distributions were: the absolute mean (μ^*, Eq. 1) and the standard deviation (σ, Eq.2) (see e.g. Saltelli et al. (2004) and Campolongo et al. (2007)). μ^* estimates the input factor influence on the output and σ assesses the ensemble of higher order factor effects on the output, i.e. nonlinear effect and/or interactions among factors. Relatively low μ^* and σ values refer to negligible effects, high μ^* and low σ values indicate linear and additive effects, and low μ^* and high σ values are the nonlinear or interactions effects. The method is composed of individually randomized OAT screening experiments which consist of varying one factor at a time and measuring the

variance of the output. Each model input factor is presumed to be varied across *p* selected levels in the input factor space. In this case study, the input factor variation for each factor was set at ±20% of the initial conditions, through 4 *p* levels. GSA was performed for the 4 experimental periods described in Section 2.2. A GSA based on these 4 periods gave a wider variability range in the environmental factors.

$$\mu_i^* = \frac{\sum_{n=1}^{r} |SEE_n|}{r} \quad (1)$$

$$\sigma_i = \sqrt{\frac{1}{r}\sum_{n=1}^{r}(SEE_n - \mu_i)^2} \quad (2)$$

where *r* is the number of repetitions of EE calculation, SEE_i is the scaled elementary effect and μ is the mean.

The software used for the GSA was the MATLAB/Simulink platform. The total number of simulations required in Morris's method is denoted as N and is calculated from Eq. 3:

$$N = r(k + 1) \quad (3)$$

where *r* is the number of repetitions of EE calculation and *k* is the input factor number.

Croop & Braddock (2002) established that a good choice of *r* is critical to obtain a good estimation of the effects. In the model developed, an *r* = 100 setting was sought with a constant resolution of *p* = 4 (Campolongo et al., 1999). The input factor values used are listed in Table 3, resulting in *k* = 34, so that the overall model evaluation costs were 3500 simulations.

The effects of these input factors were evaluated with respect to three model outputs: S_{NHx}, S_{PO4} and X_{ALG} concentrations. The simulation time period was set at 7 days to reach a pseudo-steady state and avoid excessive simulation costs.

Table 3. Default and offline/online calibrated values for the model parameters.

Parameters	Description	Value	Unit	Source
μ_{ALG}	Maximum growth rate of X_{ALG}	1.8	d^{-1}	Calibrated
$b_{ALG,1}$	Maximum inactivation rate of X_{ALG}	0.1	d^{-1}	(Reichert et al., 2001)
$b_{ALG,2}$	Maximum decay rate of X_{ALG}	0.15	d^{-1}	Calibrated
q_{XPP}	Rate constant for storage of $X_{PP\text{-}ALG}$	0.01	d^{-1}	Calibrated

K_{O2}	Half saturation parameter for S_{O2}	0.2	g O_2 m^{-3}	(Reichert et al., 2001)
$K_{Ig,C}$	Half saturation parameter for $S_{Ig,C}$	$4.32 \cdot 10^{-3}$	g C m^{-3}	(Solimeno et al., 2015)
K_{NHX}	Half saturation parameter for S_{NHX} in a phosphorus-replete medium	0.1	g N m^{-3}	Calibrated
$K_{NHX\text{-}qXPP}$	Half saturation parameter for S_{NHX} in a phosphorus-deplete medium	3	g N m^{-3}	Calibrated
K_{NO3}	Half saturation parameter for S_{NO3}	12.61	g N m^{-3}	(Wágner et al., 2016)
η_{NO3}	Reduction factor for X_{ALG} growth of S_{NO3}	0.59	–	(Eze et al., 2018)
K_{PO4}	Half saturation parameter for S_{PO4}	0.05	g P m^{-3}	Calibrated
$K_{I,PO4}$	Inhibition parameter for $X_{PP\text{-}ALG}$ use in a phosphorus-replete medium	0.15	g P m^{-3}	Calibrated
K_{XPP}	Half saturation parameter of X_{ALG} growth for $X_{PP\text{-}ALG}$	0.0027	g P m^{-3}	(Ruiz-Martinez et al., 2014)
K_{XPP_qXPP}	Half saturation parameter of X_{PP} storage for $X_{PP\text{-}ALG}$	0.003	g P m^{-3}	(Ruiz-Martínez et al., 2015)
n	Regulation coefficient or Hill number	0.006	–	(Ruiz-Martínez et al., 2015)
K_{Mg}	Half saturation parameter for S_{Mg}	0.13	g Mg m^{-3}	(Sydney et al., 2010)
K_K	Half saturation parameter for S_K	8.78	g K m^{-3}	(Sydney et al., 2010)
T_{MIN}	Minimum temperature for microalgae growth	2	°C	Calibrated
T_{MAX}	Maximum temperature for microalgae growth	40	°C	Calibrated
b	Intrinsic model parameter	87.13	–	Calibrated
c	Intrinsic model parameter	1.46	–	Calibrated
I_{OPT}	Optimal light intensity for X_{ALG} growth	230	µmol m^{-2} s^{-1}	Calibrated
k_w	Attenuation coefficient due to water	1.97	m^{-3}	(Sun et al., 2016)
K_I	Attenuation coefficient due to particulate components	0.025	m^2 g TSS^{-1}	Calibrated
$K_{I,H}$	Lower half saturation parameter for S_H	0.00001	mol H^+ L^{-1}	(Siegrist et al., 1993)
$K_{S,H}$	Upper half saturation parameter for S_H	0.00063	mol H^+ L^{-1}	(Siegrist et al., 1993)
$S_{H,opt}$	Optimal pH for X_{ALG} growth	7.50	pH	Calculated
$K_{La,O2}$	Mass transfer coefficient for oxygen	16.2	h^{-1}	Calibrated
$K_{La,CO2}$	Mass transfer coefficient for dioxide carbon	16.2	h^{-1}	Calibrated
$K_{La,NH3}$	Mass transfer coefficient for free ammonia	16.2	h^{-1}	Calibrated
k	Constants of mass transfer coefficient equation	0.05	-	Calibrated
r	Constants of mass transfer coefficient equation	1	-	Calibrated
F_{XI}	Fraction of X_I generated microalgae decay	0.25	g COD g COD^{-1}	Calculated

F_{SI}	Fraction of S_I generated microalgae decay	0.6	g C g COD^{-1}	Calculated

A more precise description of the GSA method applied in this study can be found elsewhere (Robles et al., 2014a).

2.4. Model calibration

The model was calibrated preferably with data from photo-respirometric tests and MPBR performance (offline calibration), and alternatively matching model predictions to dynamic experimental MPBR data (online calibration). Offline and online calibration were only applied to determine the values of the most influential model input factors (influential GSA factors). The rest of the input factors were set to their default values (Table 3) based on expert knowledge and the scientific literature.

2.4.1. Offline calibration

2.4.1.1. Photo-respirometric test

Offline calibration consisted of isolating specific microalgae biomass processes and measuring Oxygen Production Rate (OPR) and Oxygen Uptake Rate (OUR). Photo-respirometric tests were made to calibrate the model factors related to environmental conditions, i.e. light intensity and thermal factor. For this, a respirometer system was set up consisting of: a conical flask bioreactor (500 mL transparent glass flask), a dissolved oxygen probe (WTW CellOx 330i) recording both dissolved oxygen and temperature data every 30 s, an on-off electrovalve to add pure carbon dioxide to set pH at 7.5 and to avoid inorganic carbon limitation, a cooling-heating system connected to a heating coil for temperature control, a LED lighting system (SevenON LED 8 x 11W), and a magnetic stirrer system running at 100 rpm to ensure homogeneous conditions, prevent microalgae sedimentation, and minimize the oxygen mass transfer. The following protocol was conducted:

1. Microalgae biomass was collected from the MPBR pilot plant. Samples were centrifuged at 5000xg (Eppendorf AG 22331, Hamburg) and resuspended with AnMBR effluent to set OD_{680} at a fixed interval ranging from 0.4 to 0.6, giving comparable biomass light attenuation and nutrients concentration. An aliquot of 500 mL was transferred into the photo-respirometric system.

2. Dissolved oxygen concentration was monitored online in two differentiated phases: light and dark. The light phase was set to 20 min and the dark phase to 10 min. In the light phase, oxygen production was expected due to photosynthesis, but oxygen was also consumed due to respiration of microalgae and other possible aerobic organisms. In the dark phase the bioreactor was covered to ensure darkness and that OUR was only due to microalgae and aerobic organism respiration. The net oxygen production rate (nOPR) was thus the result of the following contributions (Eq. 4):

$$\mathrm{nOPR} = \mathrm{OPR} - \mathrm{OUR} \quad (4)$$

Different temperature (10, 20.5, 25, 30, 35 and 40 ºC) and light conditions (87, 172, 229, 314, 374, 462, 534 and 607 µmol m^{-2} s^{-1}) were tested, all runs performing under non-limiting nutrients concentration. Each temperature test (6 bioreactors) was acclimatized for 24 hours at the selected temperature and at a reference light intensity of 229 µmol m^{-2} s^{-1}. Each light intensity test (8 bioreactors) was acclimatized for 24 hours at the selected light intensity and at a reference temperature of 25 ºC. Temperature and light intensity were calibrated in triplicate, i.e. 18 and 24 trials were conducted to calibrate the effect of both temperature and light intensity on oxygen production, respectively.

The experimental nOPR was matched by the following mathematical models to calibrate cardinal temperatures (Ratkowski model) and light intensity (Steele model) using the Solver tool in Microsoft Excel. The Ratkowski model was used to describe the temperature dependence of biokinetics and to obtain the two cardinal temperatures (minimum and maximum), together with the thermic factor (F_T), which modifies kinetic rates (Eq. 5).

$$F_T = (b \cdot (T_0 - T_{MIN}))^2 \cdot (1 - e^{c \cdot (T_0 - T_{MAX})}) \quad (5)$$

where T_0 [ºC] is the culture medium temperature; T_{MIN} [ºC] is the lowest limiting temperature for growth and the expected growth rate below which is zero; b is a model parameter; T_{MAX} [ºC] is the upper temperature limit above which the expected growth rate is zero; and c is a model parameter allowing the model to fit the data at a temperature approaching and exceeding the optimum temperature for growth.

The light factor (F_L) included in light-dependent model processes was calculated by Steele's function (Eq. 6), which was selected for modeling microalgae growth according to light intensity because it includes photoinhibition and the shallow effect in photobioreactors (Steele, 1965):

$$F_L = \frac{I_{AV}}{I_{OPT}} \cdot e^{\left(1-\frac{I_{AV}}{I_{OPT}}\right)} \quad (6)$$

where I_{OPT} [µmol m^{-2} s^{-1}] is the optimal light intensity and I_{AV} [µmol m^{-2} s^{-1}] is the average light intensity. I_{AV} was obtained using Lambert-Beer's Law. The incident light intensity is attenuated by TSS [g TSS m^{-3}] concentration in the photobioreactor depth [m] (Eq. 7).

$$I_{AV} = \frac{I_{0,s} \cdot \left(1 - e^{-(k_w + K_I \cdot TSS) \cdot d}\right)}{(k_w + K_I \cdot TSS) \cdot d} \quad (7)$$

where $I_{0,s}$ [µmol m^{-2} s^{-1}] is the incident light intensity and k_w [m^{-3}] is the attenuation coefficient due to water, K_I [m^2 $gTSS^{-1}$] is the extinction coefficient associated to particulate components and d is the photobioreactor depth [m].

2.4.1.2. MPBR pilot plant

As in Ruiz et al. (2013), the PBRs were operated in two successive stages: batch and continuous operation. After microalgae inoculation with the AnMBR effluent, the PBR culture was grown in batch stage until the pseudo-stationary phase was reached (according to TSS), obtaining the batch growth kinetics and achieving a high microalgae biomass concentration. The batch stage datasets were calibrated by matching experimental data with two models: the Verhulst logistic kinetic model and Michaelis-Menten expression rate. Experimental data were matched to the corresponding model by minimizing the sum of squared residuals using Microsoft Excel Solver.

The Verhulst logistic kinetic model (Verhulst, 1838) was used to describe the PBR microalgae growth curve under batch operation and to obtain the kinetic growth factors. This model is a substrate-independent equation widely used to describe biomass growth in ecological studies, mainly because it can accurately describe biomass evolution under different culture conditions using a simple mathematical and biological definition. According to the Verhulst model, biomass growth can be expressed as sinusoidal (Eq. 8):

$$\frac{\partial X}{\partial t} = \mu_{max} X[1 - \frac{X}{X_{max}}] \quad (8)$$

285

286 Integrating Eq. 8, Eq. 9 was derived, where μ_{max} is the maximum specific growth rate [d^{-1}], X_0, X_{max} and X
287 are biomass concentrations [g VSS m^{-3}] at an operating time equal to zero, infinity and t, respectively.

$$X = \frac{X_0 X_{max} e^{t\mu_{max}}}{X_{max} - X_0 + X_0 e^{t\mu_{max}}} \quad (9)$$

288

289 The Michaelis-Menten relationship (Eq. 10) is an ecological model which can be applied to nutrient removal
290 kinetics (Aslan and Kapdan, 2006):

$$r_0 = \frac{r_{max} S_0}{K_m + S_0} \quad (10)$$

291

292 where r_0 is the nutrients uptake rate [g m^{-3} d^{-1}], r_{max} is the maximum removal rate of nutrients [d^{-1}], S_0 is the
293 nutrient concentration at time equal zero [g m^{-3}] and Km is the Michaelis-Menten constant [g m^{-3}]. The kinetic
294 coefficients r_{max} and Km were fitted and calibrated by use of the Lineweaver-Burk equation (Eq. 11).

$$\frac{1}{r_0} = \frac{K_m}{r_{max}} \frac{1}{S_0} + \frac{1}{r_{max}} \quad (11)$$

295 **2.4.2. Online calibration**

296 Online calibration with mid-term pseudo-steady periods consisted of matching the modeling results to the
297 experimental data and entailed 35 days of dynamics in nitrogen, phosphorus, VSS and sCOD concentration
298 obtained from the MPBR system. The 0.10-m wide PBR was operated with an HRT and BRT of 1.25 ± 0.03
299 and 4.5 ± 0.2 days, respectively. Medium temperature and incident PAR were 25.6 ± 1.4 ºC and 290 ± 47
300 µmol m^{-2} s^{-1}, respectively. This period was long enough to enable the effect of both phosphorus-starved and
301 -replete culture conditions. From this data, different model factors ($b_{ALG,2}$, $K_{NHX\text{-}QPP}$, $K_{I,PO4}$ and K_La) were
302 adjusted using the Matlab® Curve Fitting App. To compare and determine whether there was a significant
303 difference between the experimental data and the modeling results, the t-test and F-test, and a non-
304 continuous level test (i.e. the Mann-Whitney U-test) were performed on Statgraphics® Centurion v.19.

A mass transfer coefficient K_La function (Eq. 12) was used to describe gas transport between liquid and gas phases.

$$K_La = k \cdot \left(\frac{G_F}{V_L}\right)^r \quad (12)$$

where G_F is the gas flow rate (L h^{-1}), V_L is the liquid volume (L) and *k* and *r* are fitting parameters. Constants k (K_La_k) and r (K_La_r) were therefore the input factors calibrated to match simulated results.

2.4.3. Dynamic optimization

After offline/online calibration of the influential factors, these parameters were dynamically optimized to improve model performance throughout each experimental period. The optimization algorithm aimed at matching experimental data with the modeled results, using a standardized residuals function (Eq. 13) as objective function to be minimized. To this aim, a constrained optimization using genetic algorithm (GA) was applied through the function implemented on Matlab® software. Specifically, a global GA optimization was conducted for a predefined set of lower and upper bounds on the design variables, i.e. the influential model input factors. Bound constraints for variations of model inputs were set to ±20%. The influencing factors were fed to the GA with the same order of magnitude (unity) and later reconverted in the model function, e.g. optimal light intensity for X_{ALG} growth was 230 µmol m^{-2} s^{-1}, then a 10^{-2} factor was applied for seeding the GA; and µALG was 1.8 d^{-1}, so that it was not necessary to apply a correction factor. The termination tolerance on fitness function value ("TolFun" option) was set to 10^{-3} (it was confirmed for a given experimental period (Period 1) that the optimized results did not vary statistically when this option was reduced from 10^{-3} to 10^{-6}).

$$\sum \frac{\left|S_{NHx_{sim}} - S_{NHx_{exp}}\right|}{\sqrt{\text{std}\left(S_{NHx_{exp}}\right)}} + \sum \frac{\left|S_{PO4_{sim}} - S_{PO4_{exp}}\right|}{\sqrt{\text{std}\left(S_{PO4_{exp}}\right)}} + \sum \frac{\left|X_{ALG_{sim}} - X_{ALG_{exp}}\right|}{\sqrt{\text{std}\left(X_{ALG_{exp}}\right)}} \quad (13)$$

Bound constraints for variations of model inputs were set to ±20% of default or offline/online calibrated values.

2.5. Uncertainty analysis

UA was conducted to assess the propagation of different uncertainty sources to the model output. Only the influential input factors were considered during UA implementation, while non-important factors were set to

328 their default values. 3500 Monte Carlo runs were performed with a 20% variance rate of the influencing
329 factors. The Latin hypercube sampling method was used to generate the matrix for the Monte Carlo runs.
330 The matrix for the Monte Carlo simulations was generated using the "maximin" criteria from Matlab®
331 software, which maximize minimum distance between points. To try to optimize the Latin hypercube
332 sampling design, the default number of interactions to be applied during the Monte Carlo design was
333 increased from 5 to 100.
334 Results were assessed on different indices: (i) the 5th and 95th percentiles (Mannina et al., 2017), (ii) the p-
335 factor (Yang et al., 2008), (iii) the r-factor (Mannina et al., 2018; Yang et al., 2008) and (iv) the Average
336 Relative Interval Length (ARIL) (Mannina et al., 2018; Yang et al., 2008).

337 The p-factor, or the percentage of observations within the 95% prediction uncertainty (95PPU). The 95PPU
338 was calculated at the 2.5% and 97.5% levels of the cumulative distribution of the model output. The closer
339 the p-factor approaches 100%, the lower the uncertainty of the model predictions (Mannina et al., 2018;
340 Yang et al., 2008). The r-factor was calculated from Eq. 14 (Mannina et al., 2018; Yang et al., 2008). The
341 closer the r-factor is to 1, the narrower the uncertainty bands are.

$$\mathrm{r-factor} = \frac{\frac{1}{\mathrm{n}}\sum_{\mathrm{i=1}}^{\mathrm{n}}\left(\mathrm{y_{sim,97.5\%,i}} - \mathrm{y_{sim,2.5\%,i}}\right)}{\sigma_{\mathrm{obs}}} \quad (14)$$

342 where $y_{sim,97.5\%,i}$ and $y_{sim,2.5\%,i}$ are the upper and lower boundary value of 95PPU, respectively; n is the number
343 of observation; and σ_{obs} represents the standard deviation of the measured data.

344 The ARIL index was calculated according to Eq. 15 (Jin et al., 2010). The lower the ARIL value the lower
345 the model uncertainty.

$$\mathrm{ARIL} = \frac{1}{n}\sum_{i=1}^{n}\frac{\left(\mathrm{y_{sim,97.5\%,i}} - \mathrm{y_{sim,2.5\%,i}}\right)}{\mathrm{y_{obs}}} \quad (15)$$

346 The model uncertainty was assessed by combining the indices described above. High p-factor values, an r-
347 factor values close to 1 and low ARIL values indicate low uncertainty in the model's prediction.

3. Results and discussion

3.1. Global sensitivity analysis

3.1.1. S_{NHX} output

S_{NHX} concentration decreases due to microalgae uptake for growth and S_{NH3} stripping. Conversely, S_{NHX} concentration increases due to microalgae lysis and endogenous respiration. Processes 1 (X_{ALG} growth on S_{NHX} and S_{PO4}), 3 (X_{ALG} growth on S_{NHX} and X_{PP-ALG}), 6 (X_{ALG} endogenous respiration), 7 (X_{ALG} lysis) and 11 ($S_{[NH3]}$ stripping) in Table 1 therefore affect S_{NHX} concentration.

Figure 1 gives the sensitivity measurements (μ* and σ) calculated from each input factor on the S_{NHX} output for the 4 periods.

Maximum growth rate of X_{ALG} (μ_{ALG}), optimal light intensity (I_{OPT}) and maximum temperature (T_{MAX}) were the most sensitive input factors for Period 1 (Figure 1A). Specifically, μ_{ALG} ($\mu^* = 4.31$, $\sigma = 1.09$), I_{OPT} ($\mu^* = 2.99$, $\sigma = 0.75$) and K_I ($\mu^* = 1.72$, $\sigma = 0.50$) exhibited a linear and additive effect on S_{NHX} output, while T_{MAX} ($\mu^* = 1.68$, $\sigma = 1.31$) showed a nonlinear effect. S_{NHX} model output was mainly influenced by environmental factors, i.e. light intensity and temperature, which had a direct effect on photosynthesis and thus on net microalgae growth rate. This model output was also sensitive, although to a lesser extent, to the following input factors: K_{NHX}, $b_{ALG,2}$, K_{PO4}, $K_{I,PO4}$, $b_{ALG,1}$, $K_{NHX-QPP}$, K_{XPP}, q_{XPP} and K_La,r. All these influential input factors were involved in microalgae growth and decay rate, except K_La,r which refers to free ammonia stripping.

GSA results for S_{NHX} in Period 2 are represented in Figure 1B. Similar results to the ones obtained in Period 1 were observed in Period 2: μ_{ALG} ($\mu^* = 11.58$, $\sigma = 2.40$) and I_{OPT} ($\mu^* = 6.80$, $\sigma = 1.26$) showed a linear effect, while T_{MAX} ($\mu^* = 6.58$, $\sigma = 7.32$) exhibited a nonlinear or interactive effect on S_{NHX} output. However, the fundamental difference between the two periods was in the factors described as less influential. Whereas in Period 1 input factors related to nutrient uptake, such as half saturation constants or maximum phosphate uptake rate, had a relatively important effect on the model output, in Period 2 only one minor input, K_I ($\mu^* = 4.68$, $\sigma = 0.93$), was identified. This difference between the GSA results could be due to the available S_{NHX} concentration in the culture medium. The S_{NHX} concentrations in Periods 1 and 2 were 16 ± 6 mg N L^{-1} and 34 ± 4 mg N L^{-1}, respectively. The determination of S_{NHX} removal rate depends on external nitrogen concentrations. At high S_{NHX} concentrations, microalgae should remove ammonium-ammonia species at the

maximum rate (r_{MAX}); thus, despite increasing the substrate concentration, the removal rate will not vary where the Michaelis-Menten equation becomes independent of S_{NHX} concentration, so that the Michaelis-Menten kinetics factors were irrelevant in Period 2. As mentioned previously, the reduced S_{NHX} concentration in the culture medium was mainly due to the growth of microalgae. Growth kinetics were dependent on the global computation of the nutrients uptake, including phosphorus sources (S_{PO4} and X_{PP-ALG}). Given that microalgae growth was limited in Period 1 by the S_{NHX} concentration, input factors involved in nutrient uptake had a relatively significant effect in Period 1 as compared to Period 2.

Period 3 was operated in P-starved conditions. The GSA results from this period are reported in Figure 1C. μ_{ALG}, (μ^* = 5.28, σ = 1.49) had a relatively higher influence than the remaining input factors and a nonlinear or interactive effect on S_{NHX} model output. I_{OPT} (μ^* = 2.71, σ = 0.92) and T_{MAX} (μ^* = 1.84, σ = 0.98) presented a linear or additive effect on the model output. K_I, K_{XPP}, K_{PO4}, $K_{NHX-qPP}$, $b_{ALG,2}$, and $K_{I,PO4}$ were included in the factors classified as influential, but to a lesser extent.

GSA results for Period 4 are shown in Figure 1D. As this figure shows, there was a significant dependence of S_{NHX} concentration on microalgae growth rate, light intensity and temperature. μ_{ALG} (μ^* = 8.88, σ = 1.55), I_{OPT} (μ^* = 6.09, σ = 1.25) and K_I (μ^* = 5.39, σ = 1.25) exhibited linear or additive effects, while T_{MAX} (μ^* = 6.96, σ = 6.43) showed nonlinear or interactive effects on the output. K_La_r (μ^* = 3.21, σ = 1.65) reflected that free ammonia stripping participated on S_{NHX} concentration balance, but to a lesser degree than microalgae growth.

Regarding S_{NHX}, 10 input factors were selected as influential. Among these factors, μ_{ALG}, I_{OPT} and T_{MAX} had the greatest influence on S_{NHX} model output with linear/additive or nonlinear/iterative effects. Indeed, the variation in S_{NHX} concentration was mainly due to light-affected processes (photosynthetic metabolism), since I_{OPT} is one of the most influential input factors in S_{NHX} output. K_I was a relatively influential factor on model output in the 4 periods studied because of its intrinsic relationship to the light intensity available for photosynthesis. On the other hand, the following factors were considered as influential due to their effect on the model output within two or more periods: K_{NHX}, $b_{ALG,2}$, K_La,r, K_{PO4}, $K_{I,PO4}$ and $K_{NHX-QPP}$.

400 According to the results of the S_{NHX} model output evaluation, it would thus be recommendable to calibrate
401 the following model factors: μ_{ALG}, I_{OPT}, T_{MAX}, K_I, K_{NHX}, $b_{ALG,2}$, K_La,r, K_{PO4}, $K_{I,PO4}$ and $K_{NHX\text{-}QPP}$.

402 [FIGURE 1 NEAR HERE]

403 Figure 1. Sensitivity measures μ^* versus σ for the model outputs S_{NHX} for Period 1 (A), Period 2 (B), Period 3 (C) and Period 4 (D).

404 **3.1.2. S_{PO4} output**

405 S_{PO4} decreases due to microalgae uptake for growth and $X_{PP\text{-}ALG}$ storage. Conversely, S_{PO4} concentration
406 increases due to microalgae endogenous respiration and $X_{PP\text{-}ALG}$ and microalgae lysis. Processes 1 (X_{ALG}
407 growth on S_{NHX} and S_{PO4}), 2 (X_{ALG} growth on S_{NO3} and S_{PO4}), 5 ($X_{PP\text{-}ALG}$ storage), 6 (X_{ALG} endogenous
408 respiration) and 7 (X_{ALG} lysis) in Table 1 thus affect S_{PO4} concentration.

409 Figure 2 gives the sensitivity measurements (μ^* and σ) calculated from each input factor on the S_{PO4} output
410 for the 4 periods.

411 Seven input factors were determined as influential on S_{PO4} output. The most influential input factors for
412 Period 1 were: T_{MAX} (μ^* = 0.15, σ = 0.15) exhibiting a nonlinear or interactive effect, and q_{XPP} (μ^* = 0.24, σ
413 = 0.11), I_{OPT} (μ^* = 0.20, σ = 0.10) and K_I (μ^* = 0.11, σ = 0.07) with a linear or additive effect on the model
414 output. Contrary to S_{NHX} model output, microalgae growth processes were not the main pathway for S_{PO4}
415 removal, since polyphosphate storage also affected S_{PO4} concentration. Figure 2A discloses a higher μ^*
416 value of q_{XPP} (0.24) than μ_{ALG} (0.06), showing that S_{PO4} output was more influenced by the $X_{PP\text{-}ALG}$ storage
417 process than direct microalgae growth from S_{PO4} in Period 1. μ_{ALG}, $b_{ALG,2}$, and K_{PO4} were encompassed
418 within the input factors cluster with a relatively minor influence in the model output.

419 Period 2 (Figure 2B) highlighted T_{MAX}'s nonlinear or interactive significant effect on the model output (μ^* =
420 0.54, σ = 0.62), while q_{XPP} (μ^* = 0.49, σ = 0.23), I_{OPT} (μ^* = 0.43, σ = 0.24), μ_{ALG} (μ^* = 0.33, σ = 0.28) and K_I
421 (μ^* = 0.25, σ = 0.15) showed a linear or additive effect. The higher μ^* of q_{XPP} than μ_{ALG} indicates that $X_{PP\text{-}}$
422 $_{ALG}$ storage had a larger overall effect on the output, as well as in Period 1.

423 The effect of negligible soluble phosphorus concentration in the culture media (phosphorus-starved
424 conditions) was assessed through Period 3 (Figure 2C). The input factors q_{XPP} (μ^* = 0.025, σ = 0.007) and
425 K_{PO4} (μ^* = 0.023, σ = 0.006) stand out, suggesting that $X_{PP\text{-}ALG}$ storage was the main S_{PO4} removal pathway

and that the storage rate was dependent on soluble phosphorus concentration, both with a nonlinear or interactive effect. S_{PO4} removal by $X_{PP\text{-}ALG}$ storage process was influenced by environmental input factors, I_{OPT} (μ^* = 0.015, σ = 0.005) and T_{MAX} (μ^* = 0.012, σ = 0.006), with a nonlinear or interactive effect. K_I (μ^* = 0.008, σ = 0.003), μ_{ALG} (μ^* = 0.006, σ = 0.004) and $b_{ALG,2}$ (μ^* = 0.006, σ = 0.002) showed a relatively low μ^* values and could suggest a less influence on the model output. S_{PO4} uptake and release by microalgae absorption and lysis was thus not significant in Period 3.

Period 4 (Figure 2D) showed a nonlinear or interactive effect of T_{MAX} (μ^* = 1.31, σ = 1.20) on S_{PO4} output. Input factors related to light availability for photosynthesis – I_{OPT} (μ^* = 0.87, σ = 0.18) and K_I (μ^* = 0.75, σ = 0.19) – exhibited a lower μ^* than T_{MAX}, indicating that Period 4 was governed by temperature fluctuations and their effect on microalgae kinetics. Figure 2D differentiates three processes involved in the S_{PO4} balance: $X_{PP\text{-}ALG}$ storage, and growth and decay of microalgae. The input factor q_{XPP} (μ^* = 0.84, σ = 0.18) concerning $X_{PP\text{-}ALG}$ storage had a linear or additive effect and a higher μ^*, suggesting that the $X_{PP\text{-}ALG}$ storage process was the main pathway for S_{PO4} removal, similarly to previous periods. The relatively low μ^* value of μ_{ALG} (μ^* = 0.42, σ = 0.10) and $b_{ALG,2}$ (μ^* = 0.26, σ = 0.09), regarding microalgae growth and decay respectively, had a negligible overall effect on model output.

Regarding S_{PO4}, 7 input factors were hence selected as influential. Among these factors, T_{MAX} had the greatest influence on S_{PO4} concentration in the PBR. Indeed, this factor influences $X_{PP\text{-}ALG}$ storage, microalgae growth, and decay processes. The GSA results obtained here suggest that S_{PO4} balance was mainly affected by $X_{PP\text{-}ALG}$ storage since q_{XPP} along with T_{MAX} were the most influential input factors on S_{PO4} model output. On the other hand, the following factors were considered as influential due to their effect on the model output within two or more periods: I_{OPT}, K_I, μ_{ALG}, K_{PO4} and $b_{ALG,2}$.

Therefore, according to GSA of S_{PO4} concentration model output, the following factors must be calibrated: T_{MAX}, q_{XPP}, I_{OPT}, K_I, μ_{ALG}, K_{PO4} and $b_{ALG,2}$.

[FIGURE 2 NEAR HERE]

Figure 2. Sensitivity measures μ^* versus σ for the model outputs S_{PO4} for Period 1 (A), Period 2 (B), Period 3 (C) and Period 4 (D).

3.1.3. X_{ALG} output

X_{ALG} decreases due to microalgae lysis and endogenous respiration. Conversely, X_{ALG} increases due to microalgae growth. Processes 1 (X_{ALG} growth on S_{NHX} and S_{PO4}), 2 (X_{ALG} growth on S_{NO3} and S_{PO4}), 3 (X_{ALG} growth on S_{NHX} and $X_{PP\text{-}ALG}$), 4 (X_{ALG} growth on S_{NO3} and $X_{PP\text{-}ALG}$), 6 (X_{ALG} endogenous respiration) and 7 (X_{ALG} lysis) in Table 1 thus affect X_{ALG} concentration.

Figure 3 shows the sensitivity measurements (μ* and σ) calculated from each input factor on the X_{ALG} output for the 4 periods.

In Period 1 (Figure 3A), four input factors represented the greatest influence on the model output: μ_{ALG} (μ^* = 153.76, σ = 37.47) and T_{MAX} (μ^* = 57.24, σ = 40.62) with nonlinear or interactive effects, and I_{OPT} (μ^* = 105.17, σ = 25.64) and K_I (μ^* = 60.50, σ = 16.12) with linear or additive effects. Microalgae growth depended firstly on μ_{ALG} and secondly on the environmental factors (temperature, light intensity, nutrients concentration, etc.) conditioning biomass growth rate. Indeed, the high μ^* for μ_{ALG} indicates that it was the input factor with the most important overall effect on the model output. The higher values of μ^* and σ for I_{OPT} suggested that microalgae growth rate was subjected to average light intensity, which is in agreement with the main growth pathway of microalgae: photosynthesis. However, although microalgae productivity was due to biomass growth, cell lysis and endogenous respiration represented by input factors $b_{ALG,2}$ (μ^* = 43.04, σ = 11.20) and $b_{ALG,1}$ (μ^* = 32.13, σ = 10.24), respectively, played a relatively minor role compared to μ_{ALG}. Influential input factors on X_{ALG} output for Period 2 were thus: μ_{ALG} (μ^* = 268.76, σ = 57.78), I_{OPT} (μ^* = 153.85, σ = 26.79), K_I (μ^* = 103.53, σ = 19.83), $b_{ALG,2}$ (μ^* = 60.44, σ = 12.06) with a linear or additive effect, and T_{MAX} (μ^* = 150.66, σ = 165.04) having a nonlinear or interactive effect.

GSA results for Period 3 are shown in Figure 3C. μ_{ALG} (μ^* = 139.71, σ = 38.41) was the input with the greatest influence on X_{ALG} model output and had a nonlinear or interactive effect. Kinetic processes were mainly affected by I_{OPT} (μ^* = 70.77, σ = 23.45) and T_{MAX} to a lesser extent (μ^* = 48.77, σ = 27.60). Period 3 provided P-starved culture conditions, which explained why input factors associated with $X_{PP\text{-}ALG}$ storage and assimilation processes (K_{XPP}, μ^* = 34.23, σ = 10.08; K_{PO4}, μ^* = 32.67, σ = 14.47; $K_{NHX\text{-}qPP}$, μ^* = 32.58, σ = 6.79; and $K_{I,PO4}$, μ^* = 31.85, σ = 13.05) stood out as relatively influential.

The influence of input factors in Period 4 followed the same pattern for nutrients removal outputs as for biomass production output. The higher μ^* of μ_{ALG} (μ^* = 246.47, σ = 41.84) indicated an important overall effect on biomass productivity. Figure 3D reports that μ_{ALG} had a linear and additive effect on X_{ALG} output, while T_{MAX} (μ^* = 199.29, σ = 182.49) had a nonlinear or interactive effect. These two input factors, μ_{ALG} and T_{MAX}, were the most influential in comparison with K_I (μ^* = 88.09, σ = 33.54), I_{OPT} (μ^* = 77.38, σ = 33.94), K_{NHX} (μ^* = 60.88, σ = 14.08) and $b_{ALG,2}$ (μ^* = 53.41, σ = 15.46) which were encompassed in the cluster of input factors with a relatively minor influence. These results suggest that the input factors related to microalgae productivity were mainly regulated by PBR temperature variations and the average available light intensity did not limit microalgae growth during Period 4.

X_{ALG} model output was sensitive to 10 inputs: μ_{ALG}, T_{MAX}, $I_{OPT,}$ K_I, $b_{ALG,2}$, K_{NHX}, K_{PO4}, and $K_{NHX\text{-}qPP}$. GSA results suggested that biomass concentration balance was dominated by microalgae growth and not by endogenous respiration and microalgae lysis. The four-kinetic rates of microalgae growth were influenced by light availability and temperature. The most influential factors related to X_{ALG} biomass concentration were thus μ_{ALG}, T_{MAX}, and I_{OPT}. The remaining factors, although they had a relative influence on X_{ALG} output, were less influential.

[FIGURE 3 NEAR HERE]

Figure 3. Sensitivity measures μ^* versus σ for the model outputs X_{ALG} for Period 1 (A), Period 2 (B), Period 3 (C) and Period 4 (D).

3.1.4. Overall GSA results

Overall, 11 of the 34 model parameters were classified as influential factors: μ_{ALG}, T_{MAX}, I_{OPT}, K_I, K_{NHX}, $b_{ALG,2}$, q_{XPP}, K_{PO4}, $K_{I,PO4}$, $K_{NHX\text{-}qPP}$, and K_La_r. The four input factors with the most important overall effect on the outputs analyzed were μ_{ALG}, q_{XPP}, T_{MAX}, and I_{OPT}. The input factor μ_{ALG} showed a strong influence on the S_{NHX} and X_{ALG} output, whereby the nitrogen and biomass concentrations in the PBRs were mainly due to microalgae growth processes. Conversely, the main phosphorus removal pathway was $X_{PP\text{-}ALG}$ storage by q_{XPP}. T_{MAX} and I_{OPT} indicated that the growth and storage kinetic rates were mainly influenced by temperature and light intensity fluctuations. The model was also sensitive to nitrogen half saturation constants, K_{NHX} and

503 $K_{NHX\text{-}qPP}$ for Period 1 and Period 3, characterized by a low nitrogen and negligible phosphorus concentration,
504 respectively.

505 **3.2. Model calibration**

506 **3.2.1. Offline calibration**

507 T_{MAX}, I_{OPT}, K_I, μ_{ALG}, K_{NHX} and K_{PO4} (Table 3) were calibrated offline using experimental data from both photo-
508 respirometric tests and the MPBR pilot plant.

509 Figure 4A shows the normalized nOPR values following a typical temperature response characterized by a
510 slow rise from cold to optimum temperature before a rapid drop for higher temperatures. The Ratkowski
511 model provided a good fit with the experimental data (variance > 94%), providing T_{MIN} and T_{MAX} values of 0
512 ± 0.01 and 40.1 ± 0.2 ºC, respectively. These results were within the range of values compiled by Bernard
513 & Rémond (2012) for 15 different algal species.

514 Figure 4B shows that Steele's equation was able to describe the normalized nOPR evolution with light
515 intensity with a variance of 95%. The light curve showed the typical increase in photosynthesis light response
516 with rising light availability and a drop at high light intensities due to photoinhibition. The calibrated optimal
517 light intensity for X_{ALG} growth and attenuation coefficient were 230 ± 30 µmol m^{-2} s^{-1} and 0.025 ± 0.002 m^2
518 g TSS^{-1}. The values reported in the literature range from 80 (Khalili et al., 2015) to 413 µmol m^{-2} s^{-1} (Barbera
519 et al., 2020). This wide variation is probably due to differences in the environmental and operating conditions
520 of the experimental set-up (Bernard, 2011) and microalgae speciation (Ouyang et al., 2010). The obtained
521 attenuation coefficient of 0.025 m^2 g TSS^{-1} was in agreement with the observations made by Ruiz-Martinez
522 et al. (2014).

523 Figure 4C shows the microalgae growth kinetic curve. The experimental data was described by the logistic
524 Verhulst model to quantify microalgae growth, resulting in a match with a variance above 99% in all
525 regressions. The average μ_{ALG} obtained was 1.8 ± 0.3 d^{-1}, similar to the rates of 2, 1.6, 1.5 and 1.6 d^{-1} used
526 by most integrated microalgae models, i.e. Reichert et al. (2001), Zambrano et al. (2016), Solimeno et al.
527 (2017), and Sánchez-Zurano et al. (2021), respectively. According to the values reported in the literature, a
528 maximum growth rate of 1.8 d^{-1} is suitable for modeling microalgae growth and development in a wastewater
529 medium.

K_{NHX} and K_{PO4} were determined by the Michaelis-Menten kinetic relationship. Experimental data from 4 batch periods were linearized by the Lineweaver-Burk function (see Figure 4D). Kinetic coefficients of S_{NHX} and S_{PO4} were determined from the intercept and the slope. The observed K_{NHX} was 0.10 ± 0.02 g N m^{-3} and K_{PO4} was 0.050 ± 0.011 g P m^{-3}. The kinetic relationship proposed was able to adjust the experimental data to the model results at a variance above 96%. The calibrated KNHX value was consistent with the 0.10 g N m^{-3} adopted by Reichert et al. (2001). Zambrano et al. (2016) and Solimeno et al. (2017) both used the value proposed by Reichert et al. (2001) for model calibration and validation. As phosphorus was not usually considered a limiting nutrient, the K_{PO4} factor was not normally included in mathematical models, which limits the comparison between K_{PO4} values in the wastewater culture medium. Reichert et al. (2001) determined a phosphorus saturation constant of 0.02 g P m^{-3} for continental water bodies.

[FIGURE 4 NEAR HERE]

Figure 4. Influence of temperature (A) and light intensity (B) on normalized oxygen production rate of microalgae, biomass growth (C) and nitrogen and phosphorus consumption linearizer by Lineweaver-Burk function. Experimental and modeled data are represented by markers and lines, respectively.

3.2.2. Online calibration and dynamic optimization

$K_{NHX-qPP}$, $K_{I,PO4}$, $b_{ALG,2}$, q_{XPP}, and K_La_r factors were calibrated online after setting the calibrated values of μ_{ALG}, T_{MAX}, I_{OPT}, K_I, K_{NHX}, and K_{PO4} using data from a 35-day pseudo-stationary operating period of the MPBR pilot plant. By means of the Curve Fitting tool implemented in Matlab® software and expert knowledge, the modeling results were matched with the experimental data. $K_{NHX-qPP}$ and K_La_r parameters were calibrated using the S_{NHX} concentration as a reference, while q_{XPP} and $K_{I,PO4}$ were calibrated from S_{PO4} and total suspended phosphorus (X_P, g P m^{-3}) concentrations. $b_{ALG,2}$ was calibrated from sCOD, X_{TSS} and X_{VSS} data. The resulting data set was calibrated by evaluating the combined effect of the following 6 model outputs: S_{NHX}, S_{PO4}, X_P, X_{TSS}, X_{VSS} and sCOD. Graphical representation of the experimental results and the modeled data obtained by the calibrated factors compiled in Table 3 are reported in supplementary material.

Ruiz-Martinez et al. (2014) reported that N removal rate was higher in P-replete than in P-starved culture conditions. $K_{NHX-QPP}$ (i.e. the half saturation parameter for S_{NHX} in a phosphorus-starved medium) was

included in the model to represent this approach. The calibrated value of $K_{NHX\text{-}QPP}$ was 3 g N m^{-3}, while that of K_{NHX} was 0.1. A higher value of the half saturation constant under P-deficient culture conditions is in agreement with the observations of Ruiz-Martinez et al. (2014). Parameters $b_{ALG,2}$ and $q_{XPP\text{-}ALG}$ were calibrated at 0.15 and 0.01 d^{-1} respectively. The $b_{ALG,2}$ calibrated value was in agreement with the range reported in the literature of 0.012 to 0.21 d^{-1} (Ruiz-Martinez et al., 2014; Wágner et al., 2016).The value obtained was in agreement with the maximum rate used by the ExPIM model (Singh et al., 2018). The fitting parameter K_La_r is physically meaningless and cannot be compared with the scientific literature.

Statistical tests were performed to find any significant differences between the experimental and simulated results.

The t-test revealed a confidence interval for the difference between the means of the experimental and modeled data from -57.50 to 58.93. As this confidence interval contains the value 0, thus it can be assumed that there is no significant difference between these means, with a confidence level of 95%. Furthermore, since the calculated p-value was 0.9808 (> 0.05), the null hypothesis cannot be rejected. The means of the experimental and modeled data thus do not differ significantly from each other.

The confidence interval of the F-test ranged from 0.77 to 1.32. Since the confidence interval contained the value of 1, it can be assumed that there are no significant differences between the standard deviations of experimental and modeled data, with a confidence level of 95%. Since the calculated p-value was 0.9562 (> 0.05), the null hypothesis cannot be rejected and the standard deviations of the experimental and modeled data can be said not to differ significantly from each other.

The p-value of the Mann-Whitney U-test was 0.9184 (> 0.05), so that the null hypothesis cannot be rejected either and it can be assumed that there are no statistically significant differences between the medians of the experimental and modelled data, at a 95% confidence level.

Although, the statistical tests revealed the goodness of the results obtained with the offline/online calibration, it was decided to carry out a dynamic optimization of the 11 most influencing factors (μ_{ALG}, T_{MAX}, I_{OPT}, K_I, K_{NHX}, $b_{ALG,2}$, q_{XPP}, K_{PO4}, $K_{I,PO4}$, $K_{NHX\text{-}qPP}$ and K_La_r), to see if it was possible to obtain even better results for each period. The remaining factors were set to default values (Table 3).

583 Table 4 shows the calibrated values by offline/online methods, the dynamically optimized values for each
584 operating period, and the rounded values of optimized parameters. The model accurately predicted
585 microalgae performance using the calibrated offline/online values: an adequate correlation coefficient (R2)
586 of 0.9954 was obtained between the experimental and simulated data. It also obtained the following
587 correlation coefficients (R2) when using the optimized values: 0.9969, 0.9980, 0.9976 and 0.9982 for
588 Periods 1, 2, 3 and 4, respectively (average R2 of 0.9977). The model accuracy using the sets of model
589 parameters values obtained from both the offline/online calibration and the dynamic optimization was also
590 assessed by Root Mean Square Error (RMSE) and Sum of Squares due to error (SSE). RMSE and SSE
591 were reduced by 47% and 27%, respectively, when using the dynamically optimized values for the model
592 parameters over the offline/online calibrated ones.
593 The model performance can thus be said to have only slightly improved by dynamically optimizing the
594 model's influential parameters, validating the values obtained from the offline/online calibrated values from
595 experimental data.

596 Table 4. Offline/online calibrated and dynamically optimized values for the influential model parameters. SD was not specified in
597 online and dynamically calibrated factors because they were set to a single specific value.

Parameter		Offline/Online Calibrated value	Dynamic Optimization values				
			Period 1	Period 2	Period 3	Period 4	Mean ± SD
μ_{ALG}	d^{-1}	1.8 ± 0.3[1]	1.63	1.45	2.14	2.00	1.8 ± 0.3
K_{NHX}	g N m^{-3}	0.10 ± 0.02[1]	0.11	0.12	0.095	0.10	0.109 ± 0.012
$K_{NHX-QPP}$	g N m^{-3}	3[2]	3.55	3.57	2.54	3.56	3.3 ± 0.5
K_{PO4}	g P m^{-3}	0.050 ± 0.011[1]	0.04	0.05	0.04	0.06	0.049 ± 0.008
$K_{I,PO4}$	g P m^{-3}	0.15[2]	0.17	0.12	0.13	0.12	0.14 ± 0.02
I_{opt}	µmol m^{-2} s^{-1}	230 ± 30[1]	187.47	199.23	184.78	215.56	197 ± 14
K_I	m^2 g TSS^{-1}	0.025 ± 0.002[1]	0.028	0.020	0.022	0.027	0.024 ± 0.004
T_{max}	°C	40.1 ± 0.2[1]	33.76	44.89	34.69	42.90	39 ± 6
$b_{ALG,2}$	d^{-1}	0.15[2]	0.15	0.14	0.16	0.17	0.156 ± 0.013
q_{XPP}	d^{-1}	0.010[2]	0.0096	0.011	0.011	0.012	0.0110 ± 0.0010
K_La_r	-	1[2]	0.86	1.00	1.19	0.81	1.0 ± 0.2

598 [1]Offline calibrated
599 [2]Online calibrated
600

3.3. **Uncertainty analysis**

3.3.1. **S_{NHX} output**

The results for S_{NHX} output from Monte Carlo simulations in the 4 periods are reported as supplementary material. There were 3500 lines (spaghettis), each one referring to the results of one simulation. The varying spread of the band in the multiple probability density function plot indicated the extent of the uncertainty in the simulated S_{NHX} at different sampling times. The 5th and 95th Monte Carlo percentiles (uncertainty bands) were calculated; the further away the uncertainty bands from the mean value, the greater the uncertainty. Figure 5 shows the experimental and calibrated model results, as well as the uncertainty bands for the 4 periods. It can be seen that the uncertainty bandwidths change with the period considered. This could be due to variations in the influencing factors of each period, the role they played in the variation of the model output and the interlinkage between the model outputs. The uncertainty bandwidths can be quantified from the r-factor (Table 5). The closer the r-factor to 1, the narrower the uncertainty bands. According to this uncertainty factor, the uncertainty in Periods 3 and 4 is therefore lower than in Periods 1 and 2. UA results should be complemented with other indices such as the p-factor and the ARIL value. The closer to 100% the p-factor, the lower the uncertainty of the model predictions. Conversely, the lower the ARIL value, the lower the model uncertainty. The p-factor value was above 90% In all the periods because the wide bands obtained embrace most of the data. However, in this specific case, the large values obtained for the p-factor did not reflect low model uncertainty but rather the great width of the uncertainty bands and therefore a high degree of uncertainty. For the ARIL value (Table 5), Period 4 had the lowest uncertainty of all the remaining periods. As the uncertainty of the periods varied according to the target coefficient, it was required to combine the three uncertainty coefficients analysis together with the uncertainty bandwidth for a critical UA. Compiling the three coefficients, Period 4 showed low uncertainty (r-factor: 1.56, p-factor: 100% and ARIL: 0.22). From the 11 influential parameters, only T_{MAX} showed a strong influence on S_{NHX} output in Period 4, while the remaining factors had a relatively less influential effect, so that the model was mainly influenced by T_{MAX}, reducing the range of the simulation uncertainty bands.

A larger bandwidth and uncertainty coefficient values were obtained for Periods 1, 2 and 3 (Table 5). Four (μ_{ALG}, T_{MAX}, I_{OPT} and K_I) and 9 (μ_{ALG}, T_{MAX}, I_{OPT}, K_I, K_{NHX}, K_{PO4}, $K_{NHX\text{-}qPP}$, $K_{I,PO4}$ and $b_{ALG,2}$) of the influencing parameters were identified in Periods 2 and 3, respectively, while all of them were identified in Period 1.

Comparing the uncertainty bandwidth and coefficients obtained for the 4 periods, the results suggest that the model uncertainty is influenced by the number of influential input factors involved in each period. As expected, the more the influencing input factors involved, the greater the uncertainty of the model appears to be.

[FIGURE 5 NEAR HERE]

Figure 5. Calibrated, experimental data, 95th and 5th percentiles for S_{NHX} concentration in the MPBR effluent for Period 1 (A), Period 2 (B), Period 3 (C) and Period 4 (D).

3.3.2. **S_{PO4} output**

The results for S_{PO4} output from the Monte Carlo simulation are also reported as supplementary material. The results of the S_{PO4} model output showed the model's good response in terms of uncertainty for Periods 1, 2 and 4. Nearly all the experimental data (p-factor value > 70%) lay inside the uncertainty bands (Figure 6A, B and D, Table 5). All the experimental data obtained for Period 2 were inside the 5th and 95th percentiles with a p-factor value of 100%, because this period presented the widest bandwidth with an r-factor value of 2.10. According to the uncertainty coefficient values reported by Mannina et al. (2018), the r-factor value for Period 2 showed a degree of uncertainty in the model output, although the low ARIL value (0.69) suggested a good response of the model in terms of uncertainty.

In Periods 1 and 4, the r-factor values close to 1 (1.72 and 0.58, respectively) and the low ARIL values (0.46 and 0.11, respectively), combined with the high p-factor value (75 and 71%, respectively), suggested an acceptable model response in uncertainty terms.

In contrast to the preceding periods, Period 3 showed high uncertainty in terms of S_{PO4} output. Although most experimental data fell within the uncertainty bands (p-factor value of 86%), the high ARIL value and r-factor provided high uncertainty in the S_{PO4} output. According to GSA, the more influential input factors were related to $X_{PP\text{-}ALG}$ storage. The higher level of uncertainty than the other periods could be due to the fact that storage and assimilation of $X_{PP\text{-}ALG}$ played a more significant role in Period 3. The results suggested that the uncertainty propagation through the model output was due to parameters related to $X_{PP\text{-}ALG}$.

[FIGURE 6 NEAR HERE]

Figure 6. Calibrated, experimental data, 95th and 5th percentiles for S_{PO4} concentration in the MPBR effluent for Period 1 (A), Period 2 (B), Period 3 (C) and Period 4 (D).

3.3.3. X_{ALG} output

The results of X_{ALG} output from the Monte Carlo simulation are reported as supplementary material and the uncertainty coefficient values are shown in Table 5. In X_{ALG}, all the experimental data lay inside the uncertainty bands (Figure 7) and the p-factor was 100% for each period. As ARIL values were lower than 1, given the high p-factor values and low ARIL values, a good model response in terms of uncertainty would be obtained for the X_{ALG} output. However, the r-factor values on average were not near 1, with the closest being 2.06 in Period 3. As detailed above, the wider the bandwidth, the greater the probability of the experimental data being inside the uncertainty bands. Consequently, although the p-factor value mathematically provided low uncertainty, the model response should be analyzed as a whole, considering the overall computation of the uncertainty coefficients and Monte Carlo simulations.

[FIGURE 7 NEAR HERE]

Figure 7. Calibrated, experimental data, 95th and 5th percentiles for X_{ALG} concentration in the MPBR effluent for Period 1 (A), Period 2 (B), Period 3 (C) and Period 4 (D).

Table 5. Uncertainty coefficient for each Period and model output: p-factor, r-factor and ARIL.

Output - #Period	p-factor	r-factor	ARIL
S_{NHX} - 1	100	2.42	1.61
S_{NHX} - 2	94.44	5.70	0.73
S_{NHX} - 3	100	1.51	0.84
S_{NHX} - 4	100	1.56	0.22
S_{PO4} - 1	75.00	1.72	0.46
S_{PO4} - 2	100	2.10	0.69
S_{PO4} - 3	85.71	12.63	2.94
S_{PO4} - 4	71.43	0.58	0.11
X_{ALG} - 1	100	3.45	0.50
X_{ALG} - 2	100	4.35	0.74
X_{ALG} - 3	100	2.06	0.31
X_{ALG} - 4	100	4.49	0.65

3.3.4. **Overall uncertainty analysis**

The Monte Carlo simulation and uncertainty coefficients show different responses in terms of uncertainty for each period. This result is probably due to two main reasons: (i) the number of sensitive factors involved and (ii) the processes involved in each period. The results obtained for the S_{NHX} model output suggested that the uncertainty bandwidth depended on the number of influential input factors involved. S_{PO4} output suggested that the processes involved in each period had different effects on model output variations and on the interrelationship between model outputs. On the other hand, although p-factor and ARIL values for X_{ALG} output suggested a good response in terms of uncertainty, an integrated analysis of all uncertainty indices (bandwidth, p-factor, r-factor and ARIL value) showed high uncertainty in the model output.

The high uncertainty response of the 3 model outputs could be attributed to online calibrated factors. The reproducibility of this online calibration approach may be questionable and could introduce uncertainty into the model. The problem with online calibration is the non-identifiability of the parameters, which leads to accepting the possible "equifinality" of the models, i.e. there is no one "optimal" set of calibrated parameters to represent microalgae culture, although there are multiple combinations of parameter values for a chosen model structure that can be equally valid for matching data (Sin et al., 2005). These model parameter sets can be distributed over a wide range of values for each parameter, introducing high uncertainty into the model. Offline calibration is an alternative method to online calibration. In this respect, offline calibration enables kinetic processes to be isolated and the variables involved to be controlled. In this study, offline calibration was performed by: (i) photo-respirometry tests with biomass adapted from the MPBR pilot plant; and (ii) microalgae growth in batch conditions, so that the offline calibrated data agree with the intrinsic characteristics of microalgae culture and operating conditions and thus provide more reliable values. Since a subset of the parameters was calibrated online, an optimization algorithm was used to match the model parameters within a realistic data range. The offline method can thus be recommended over online calibration, as can the dynamic optimization of all the influential parameters.

4. **Conclusions**

This paper presents a GSA, an offline/online calibration, a dynamic optimization, and a UA of a previously proposed and validated microalgae model. Eleven out of 34 influential factor were identified from the GSA.

The four factors with the most important overall effect on the three outputs evaluated (S_{NHX}, S_{PO4} and X_{ALG}) were μ_{ALG}, q_{XPP}, T_{MAX} and I_{OPT}. S_{NHX} and X_{ALG} model outputs were influenced by kinetic input factors related to microalgae growth, while S_{PO4} model output was affected by $X_{PP\text{-}ALG}$ storage. A single data set was achieved by offline/online calibration methods able to reproduce the model outputs for the 4 experimental periods evaluated, regardless of the operational and environmental conditions. A dynamic optimization of the calibrated model parameter values was conducted to improve the model's output response. The UA results revealed different responses according to the model output and the operating period considered and were dependent on the processes and the number of influencing input factors involved in each period. Uncertainty indices were analyzed together with uncertainty bands to avoid erroneous conclusions. The model's uncertainty results revealed the need to prioritize offline calibration to improve model performance.

ACKNOWLEDGEMENTS

This research work was supported by the Spanish Ministry of Economy and Competitiveness (MINECO, Projects CTM2014-54980-C2-1-R, CTM2014-54980-C2-2-R, CTM2017-86751-C2-1-R and CTM2017-86751-C2-2-R) jointly with the European Regional Development Fund (ERDF), both of which are gratefully acknowledged. It was also supported by the Spanish Ministry of Education, Culture and Sport via a pre-doctoral FPU fellowship to author Stéphanie Aparicio (FPU/15/02595).

References

APHA, AWWA, WEF, 2005. Standard Methods for the Examination of Water and Wastewater, 21st ed, American Public Health Association. Washington, DC.

Aslan, S., Kapdan, I.K., 2006. Batch kinetics of nitrogen and phosphorus removal from synthetic wastewater by algae. Ecol. Eng. 28, 64–70. https://doi.org/10.1016/j.ecoleng.2006.04.003

Barbera, E., Sforza, E., Grandi, A., Bertucco, A., 2020. Uncoupling solid and hydraulic retention time in photobioreactors for microalgae mass production : A model-based analysis. Chem. Eng. Sci. 218, 115578. https://doi.org/10.1016/j.ces.2020.115578

Bernard, O., 2011. Hurdles and challenges for modelling and control of microalgae for CO 2 mitigation and biofuel production, in: Journal of Process Control. pp. 1378–1389. https://doi.org/10.1016/j.jprocont.2011.07.012

728 Bernard, O., Rémond, B., 2012. Validation of a simple model accounting for light and temperature effect on
729 microalgal growth. Bioresour. Technol. 123, 520–527. https://doi.org/10.1016/j.biortech.2012.07.022

730 Campolongo, F., Cariboni, J., Saltelli, A., 2007. An effective screening design for sensitivity analysis of large
731 models. Environ. Model. Softw. 22, 1509–1518. https://doi.org/10.1016/j.envsoft.2006.10.004

732 Campolongo, F., Tarantola, S., Saltelli, A., 1999. Tackling quantitatively large dimensionality problems.
733 Comput. Phys. Commun. 117, 75–85. https://doi.org/10.1016/S0010-4655(98)00165-9

734 Corominas, L., Neumann, M.B., 2014. Ecosystem-based management of a Mediterranean urban
735 wastewater system: A sensitivity analysis of the operational degrees of freedom. J. Environ. Manage.
736 143, 80–87. https://doi.org/10.1016/J.JENVMAN.2014.04.021

737 Costache, T.A., Gabriel Acien Fernandez, F., Morales, M.M., Fernández-Sevilla, J.M., Stamatin, I., Molina,
738 E., 2013. Comprehensive model of microalgae photosynthesis rate as a function of culture conditions
739 in photobioreactors. Appl. Microbiol. Biotechnol. 97, 7627–7637. https://doi.org/10.1007/s00253-013-
740 5035-2

741 Davison, I.R., 1991. ENVIRONMENTAL EFFECTS ON ALGAL PHOTOSYNTHESIS: TEMPERATURE. J.
742 Phycol. https://doi.org/10.1111/j.0022-3646.1991.00002.x

743 Eze, V.C., Velasquez-Orta, S.B., Hernández-García, A., Monje-Ramírez, I., Orta-Ledesma, M.T., 2018.
744 Kinetic modelling of microalgae cultivation for wastewater treatment and carbon dioxide sequestration.
745 Algal Res. 32, 131–141. https://doi.org/10.1016/j.algal.2018.03.015

746 González-Camejo, J., Aparicio, S., Ruano, M. V., Borrás, L., Barat, R., Ferrer, J., 2019. Effect of ambient
747 temperature variations on an indigenous microalgae-nitrifying bacteria culture dominated by Chlorella.
748 Bioresour. Technol. 290, 121788. https://doi.org/10.1016/j.biortech.2019.121788

749 González-Camejo, J., Barat, R., Aguado, D., Ferrer, J., 2020. Continuous 3-year outdoor operation of a flat-
750 panel membrane photobioreactor to treat effluent from an anaerobic membrane bioreactor. Water
751 Res. 169. https://doi.org/10.1016/j.watres.2019.115238

752 González-Camejo, J., Barat, R., Ruano, M.V., Seco, A., Ferrer, J., 2018. Outdoor flat-panel membrane

753 photobioreactor to treat the effluent of an anaerobic membrane bioreactor. Influence of operating,
754 design, and environmental conditions. Water Sci. Technol. 78. https://doi.org/10.2166/wst.2018.259

755 Jin, X., Xu, C.Y., Zhang, Q., Singh, V.P., 2010. Parameter and modeling uncertainty simulated by GLUE
756 and a formal Bayesian method for a conceptual hydrological model. J. Hydrol. 383, 147–155.
757 https://doi.org/10.1016/j.jhydrol.2009.12.028

758 Khalili, A., Najafpour, G.D., Amini, G., Samkhaniyani, F., 2015. Influence of nutrients and LED light
759 intensities on biomass production of microalgae Chlorella vulgaris. Biotechnol. Bioprocess Eng. 20,
760 284–290. https://doi.org/10.1007/s12257-013-0845-8

761 Kim, S., Lee, Y., Hwang, S.J., 2013. Removal of nitrogen and phosphorus by Chlorella sorokiniana cultured
762 heterotrophically in ammonia and nitrate. Int. Biodeterior. Biodegrad. 85, 511–516.
763 https://doi.org/10.1016/j.ibiod.2013.05.025

764 Mannina, G., Cosenza, A., Ekama, G.A., 2017. Greenhouse gases from membrane bioreactors:
765 Mathematical modelling, sensitivity and uncertainty analysis. Bioresour. Technol. 239, 353–367.
766 https://doi.org/10.1016/j.biortech.2017.05.018

767 Mannina, G., Cosenza, A., Viviani, G., Ekama, G.A., 2018. Sensitivity and uncertainty analysis of an
768 integrated ASM2d MBR model for wastewater treatment. Chem. Eng. J. 351, 579–588.
769 https://doi.org/10.1016/j.cej.2018.06.126

770 Markou, G., Vandamme, D., Muylaert, K., 2014. Microalgal and cyanobacterial cultivation: The supply of
771 nutrients. Water Res. https://doi.org/10.1016/j.watres.2014.07.025

772 Morris, M.D., 1991. Factorial sampling plans for preliminary computational experiments. Technometrics 33,
773 161–174. https://doi.org/10.1080/00401706.1991.10484804

774 Nagase, H., Yoshihara, K. ichi, Eguchi, K., Okamoto, Y., Murasaki, S., Yamashita, R., Hirata, K., Miyamoto,
775 K., 2001. Uptake pathway and continuous removal of nitric oxide from flue gas using microalgae.
776 Biochem. Eng. J. 7, 241–246. https://doi.org/10.1016/S1369-703X(00)00122-4

777 Ndiaye, M., Gadoin, E., Gentric, C., 2018. CO2 gas–liquid mass transfer and kLa estimation: Numerical

778 investigation in the context of airlift photobioreactor scale-up. Chem. Eng. Res. Des. 133, 90–102.
779 https://doi.org/10.1016/j.cherd.2018.03.001

780 Ouyang, Z.-R., Wen, X.-B., Geng, Y.-H., Mei, H., Hu, H.-J., Zhang, G.-Y., Li, Y.-G., 2010. The Effects of
781 Light Intensities, Temperatures, pH and Salinities on Photosynthesis of Chlorella. Plant Sci. J. 30, 49–
782 55. https://doi.org/10.3724/sp.j.1142.2010.00049

783 Pastore, M., Barbera, E., Panichi, A., Sforza, E., 2020. Application of photorespirometry to unravel algal
784 kinetic parameters of nitrogen consumption in complex media. Algal Res. 47, 101837.
785 https://doi.org/10.1016/j.algal.2020.101837

786 Rajabi, M.M., Fahs, M., Panjehfouladgaran, A., Ataie-Ashtiani, B., Simmons, C.T., Belfort, B., 2020.
787 Uncertainty quantification and global sensitivity analysis of double-diffusive natural convection in a
788 porous enclosure. Int. J. Heat Mass Transf. 162, 120291.
789 https://doi.org/10.1016/j.ijheatmasstransfer.2020.120291

790 Reichert, P., Borchardt, D., Henze, M., Rauch, W., Shanahan, P., Somlyódy, L., Vanrolleghem, P., 2001.
791 River Water Quality Model no. 1 (RWQM1): II. Biochemical process equations . Water Sci. Technol.
792 43, 11–30. https://doi.org/10.2166/wst.2001.0241

793 Robles, A., Ruano, M. V., Ribes, J., Seco, A., Ferrer, J., 2014a. Global sensitivity analysis of a filtration
794 model for submerged anaerobic membrane bioreactors (AnMBR). Bioresour. Technol. 158, 365–373.
795 https://doi.org/10.1016/j.biortech.2014.02.087

796 Robles, A., Ruano, M. V., Ribes, J., Seco, A., Ferrer, J., 2014b. Model-based automatic tuning of a filtration
797 control system for submerged anaerobic membrane bioreactors (AnMBR). J. Memb. Sci. 465, 14–26.
798 https://doi.org/10.1016/J.MEMSCI.2014.04.012

799 Ruano, M. V., Ribes, J., Ferrer, J., Sin, G., 2011. Application of the Morris method for screening the
800 influential parameters of fuzzy controllers applied to wastewater treatment plants. Water Sci. Technol.
801 63, 2199–2206. https://doi.org/10.2166/wst.2011.442

802 Ruano, M. V., Ribes, J., Seco, A., Ferrer, J., 2012. An improved sampling strategy based on trajectory

803 design for application of the Morris method to systems with many input factors. Environ. Model. Softw.
804 37, 103–109. https://doi.org/10.1016/J.ENVSOFT.2012.03.008

805 Ruiz-Martinez, A., Serralta, J., Pachés, M., Seco, A., Ferrer, J., 2014. Mixed microalgae culture for
806 ammonium removal in the absence of phosphorus: Effect of phosphorus supplementation and process
807 modeling. Process Biochem. 49, 2249–2257. https://doi.org/10.1016/j.procbio.2014.09.002

808 Ruiz-Martínez, A., Serralta, J., Romero, I., Seco, A., Ferrer, J., 2015. Effect of intracellular P content on
809 phosphate removal in Scenedesmus sp. Experimental study and kinetic expression. Bioresour.
810 Technol. 175, 325–332. https://doi.org/10.1016/j.biortech.2014.10.081

811 Ruiz, J., Álvarez-Díaz, P.D., Arbib, Z., Garrido-Pérez, C., Barragán, J., Perales, J.A., 2013. Performance of
812 a flat panel reactor in the continuous culture of microalgae in urban wastewater: Prediction from a
813 batch experiment. Bioresour. Technol. 127, 456–463. https://doi.org/10.1016/j.biortech.2012.09.103

814 Ruiz, J, Arbib, Z., Álvarez-Díaz, P.D., Garrido-Pérez, C., Barragán, J., Perales, J.A., 2013.
815 Photobiotreatment model (PhBT): A kinetic model for microalgae biomass growth and nutrient removal
816 in wastewater. Environ. Technol. (United Kingdom). https://doi.org/10.1080/09593330.2012.724451

817 Saltelli, A., Tarantola, S., Campolongo, F., Ratto, M., 2004. Sensitivity Analysis in Practice: A Guide to
818 Assessing Scientific Models.

819 Sánchez-Zurano, A., Rodríguez-miranda, E., Guzmán, J.L., Acién-fernández, F.G., Fernández-sevilla,
820 J.M., Grima, E.M., 2021. Abaco: A new model of microalgae-bacteria consortia for biological treatment
821 of wastewaters. Appl. Sci. 11, 1–24. https://doi.org/10.3390/app11030998

822 Seco, A., Aparicio, S., González-Camejo, J., Jiménez-Benítez, A., Mateo, O., Mora, J.F., Noriega-Hevia, G.,
823 Sanchis-Perucho, P., Serna-García, R., Zamorano-López, N., Giménez, J.B., Ruiz-Martínez, A.,
824 Aguado, D., Barat, R., Borrás, L., Bouzas, A., Martí, N., Pachés, M., Ribes, J., Robles, A., Ruano, M.
825 V., Serralta, J., Ferrer, J., 2018. Resource recovery from sulphate-rich sewage through an innovative
826 anaerobic-based water resource recovery facility (WRRF). Water Sci. Technol. 78, 1925–1936.
827 https://doi.org/10.2166/wst.2018.492

Shoener, B.D., Schramm, S.M., Béline, F., Bernard, O., Martínez, C., Plósz, B.G., Snowling, S., Steyer, J.P., Valverde-Pérez, B., Wágner, D., Guest, J.S., 2019. Microalgae and cyanobacteria modeling in water resource recovery facilities: A critical review. Water Res. X. https://doi.org/10.1016/j.wroa.2018.100024

Siegrist, H., Renggli, D., Gujer, W., 1993. Mathematical modelling of anaerobic mesophilic sewage sludge treatment, in: Water Science and Technology. pp. 25–36. https://doi.org/10.2166/wst.1993.0070

Sin, G., Gernaey, K. V., 2009. Improving the Morris method for sensitivity analysis by scaling the elementary effects. Comput. Aided Chem. Eng. 26, 925–930. https://doi.org/10.1016/S1570-7946(09)70154-3

Sin, G., Gernaey, K. V., Neumann, M.B., van Loosdrecht, M.C.M., Gujer, W., 2011. Global sensitivity analysis in wastewater treatment plant model applications: Prioritizing sources of uncertainty. Water Res. 45, 639–651. https://doi.org/10.1016/J.WATRES.2010.08.025

Sin, G., Van Hulle, S.W.H., De Pauw, D.J.W., Van Griensven, A., Vanrolleghem, P.A., 2005. A critical comparison of systematic calibration protocols for activated sludge models: A SWOT analysis. Water Res. 39, 2459–2474. https://doi.org/10.1016/J.WATRES.2005.05.006

Singh, D., Nedbal, L., Ebenhöh, O., 2018. Modelling phosphorus uptake in microalgae. Biochem. Soc. Trans. https://doi.org/10.1042/BST20170262

Solimeno, A., Parker, L., Lundquist, T., García, J., 2017. Integral microalgae-bacteria model (BIO_ALGAE): Application to wastewater high rate algal ponds. Sci. Total Environ. 601–602, 646–657. https://doi.org/10.1016/j.scitotenv.2017.05.215

Solimeno, A., Samsó, R., García, J., 2016. Parameter sensitivity analysis of a mechanistic model to simulate microalgae growth. Algal Res. 15, 217–223. https://doi.org/10.1016/J.ALGAL.2016.02.027

Solimeno, A., Samsó, R., Uggetti, E., Sialve, B., Steyer, J.P., Gabarró, A., García, J., 2015. New mechanistic model to simulate microalgae growth. Algal Res. https://doi.org/10.1016/j.algal.2015.09.008

Steele, J.H., 1965. Notes on some theoretical problems in production ecology. Goldman, C. R. (ed.), Prim. Product. Aquat. Environ. (Mem. Ist. Ital. Idrobiol., 18 Suppl.) 383–398.

853 Sun, H., Zhu, Y., Yang, J., Wang, X., 2015. Global sensitivity analysis for an integrated model for simulation
854 of nitrogen dynamics under the irrigation with treated wastewater. Environ. Sci. Pollut. Res. 2015 2221
855 22, 16664–16675. https://doi.org/10.1007/S11356-015-4860-5

856 Sun, Y., Huang, Y., Liao, Q., Fu, Q., Zhu, X., 2016. Enhancement of microalgae production by embedding
857 hollow light guides to a flat-plate photobioreactor. Bioresour. Technol. 207, 31–38.
858 https://doi.org/10.1016/j.biortech.2016.01.136

859 Sydney, E.B., Sturm, W., de Carvalho, J.C., Thomaz-Soccol, V., Larroche, C., Pandey, A., Soccol, C.R.,
860 2010. Potential carbon dioxide fixation by industrially important microalgae. Bioresour. Technol. 101,
861 5892–5896. https://doi.org/10.1016/j.biortech.2010.02.088

862 Verhulst, P.-F., 1838. Notice sur la loi que la population suit dans son accroissement. Correspondance
863 Mathématique et Physique Publiée par A. Quetelet 10, 113–121.

864 Viruela, A., Aparicio, S., Robles, Á., Falomir, L.B., Serralta, J., Seco, A., Ferrer, J., 2021. Kinetic modeling
865 of autotrophic microalgae mainline processes for sewage treatment in phosphorus-replete and -
866 deplete culture conditions. Sci. Total Environ. 149165.
867 https://doi.org/10.1016/J.SCITOTENV.2021.149165

868 Viruela, A., Robles, Á., Durán, F., Ruano, M.V., Barat, R., Ferrer, J., Seco, A., 2018. Performance of an
869 outdoor membrane photobioreactor for resource recovery from anaerobically treated sewage. J.
870 Clean. Prod. 178, 665–674. https://doi.org/10.1016/j.jclepro.2017.12.223

871 Wágner, D.S., Valverde-Pérez, B., Sæbø, M., Bregua de la Sotilla, M., Van Wagenen, J., Smets, B.F., Plósz,
872 B.G., 2016. Towards a consensus-based biokinetic model for green microalgae – The ASM-A. Water
873 Res. 103, 485–499. https://doi.org/10.1016/j.watres.2016.07.026

874 Yang, J., Reichert, P., Abbaspour, K.C., Xia, J., Yang, H., 2008. Comparing uncertainty analysis techniques
875 for a SWAT application to the Chaohe Basin in China. J. Hydrol. 358, 1–23.
876 https://doi.org/10.1016/j.jhydrol.2008.05.012

877 Zambrano, J., Krustok, I., Nehrenheim, E., Carlsson, B., 2016. A simple model for algae-bacteria interaction

878 in photo-bioreactors. Algal Res. 19, 155–161. https://doi.org/10.1016/j.algal.2016.07.022

879

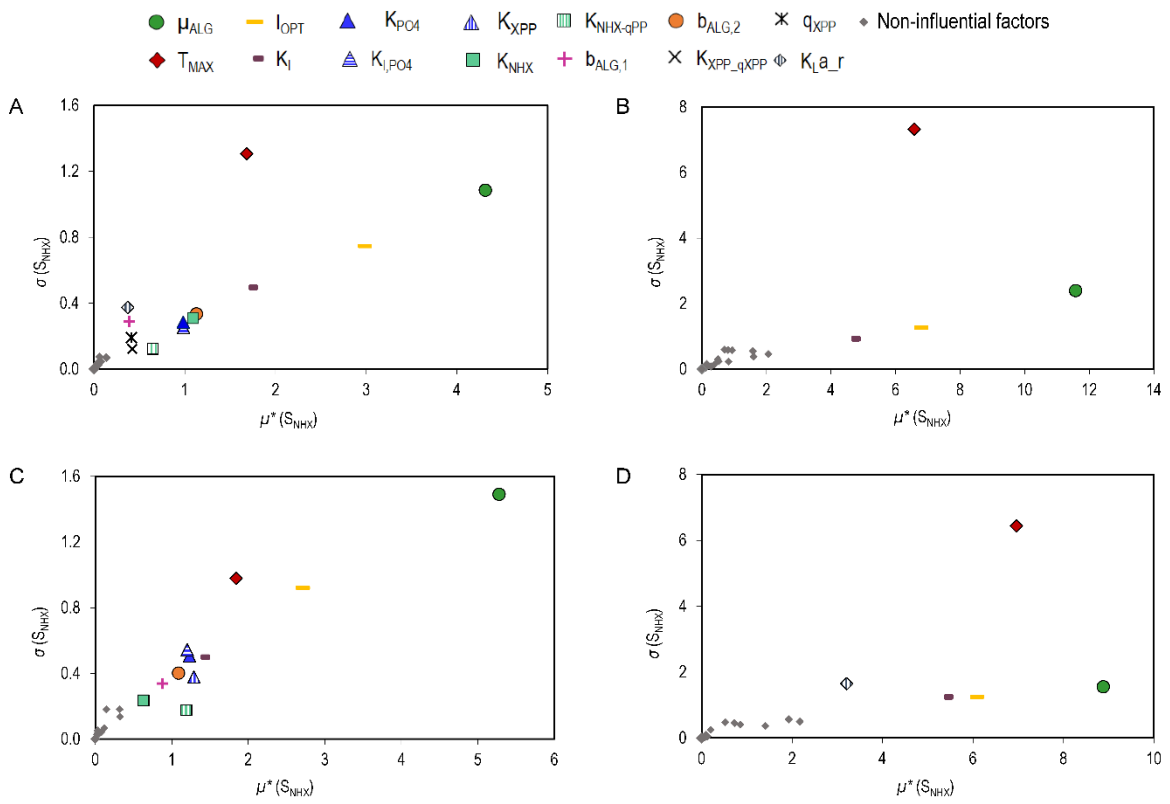

Figure 1

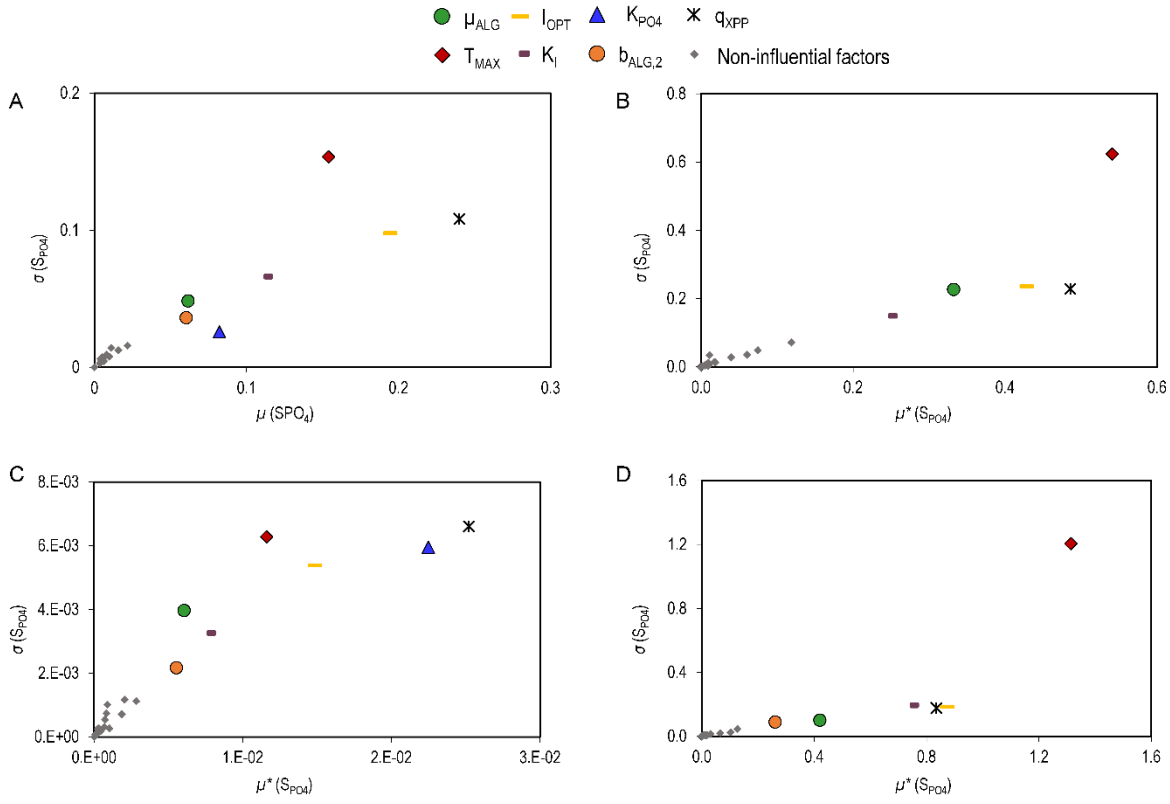

Figure 2

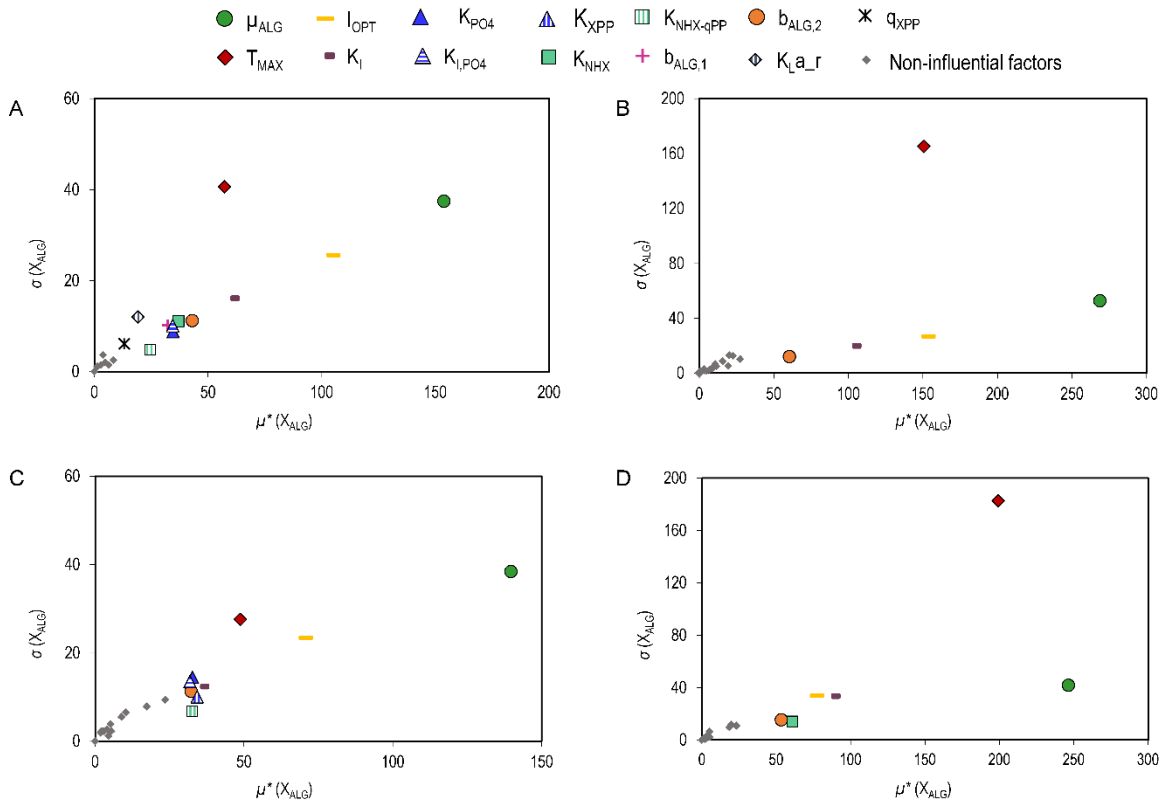

Figure 3

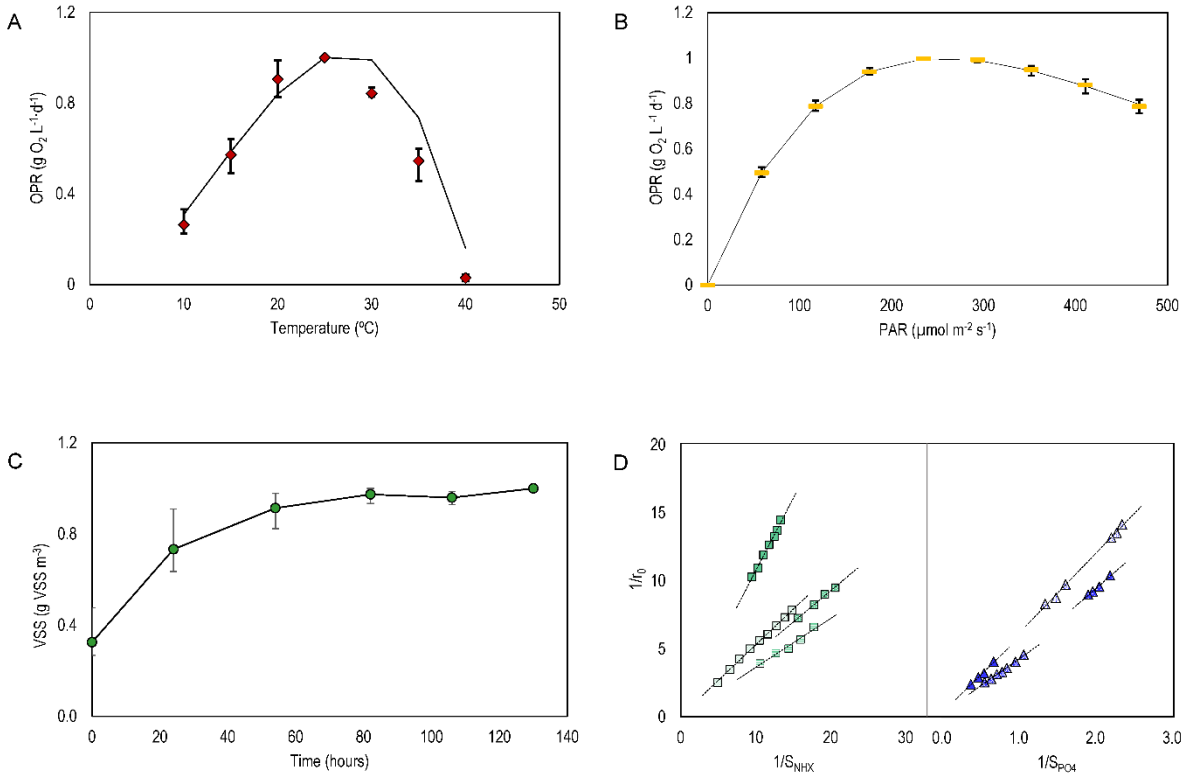

Figure 4

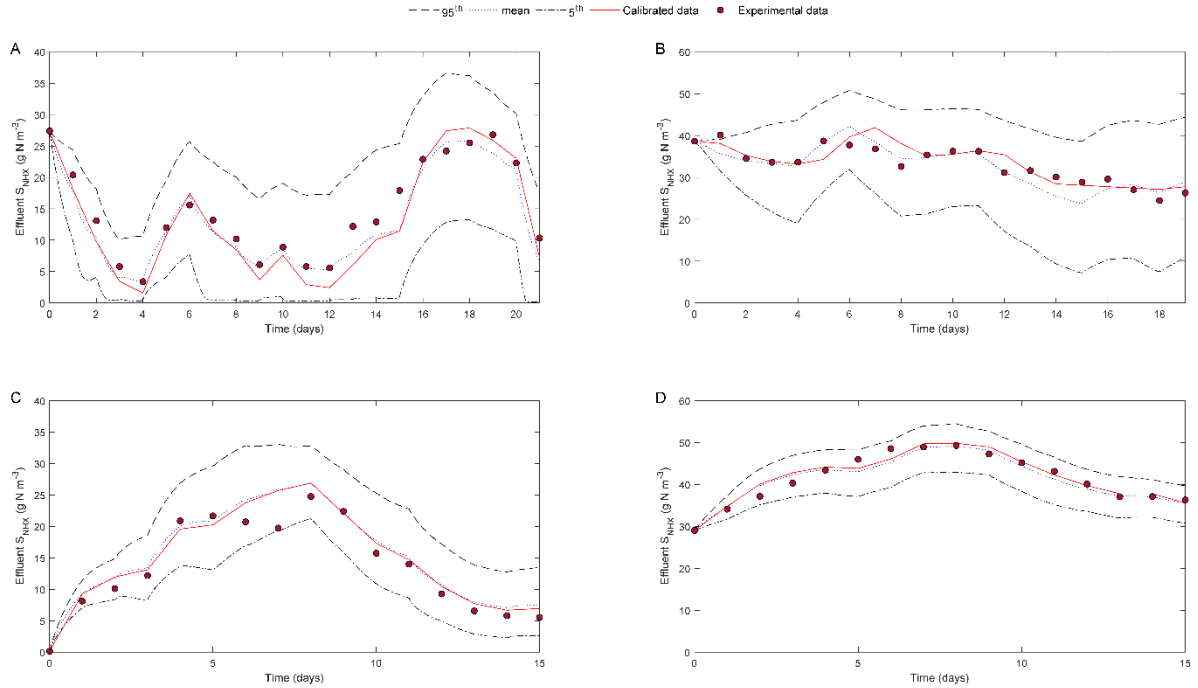

Figure 5

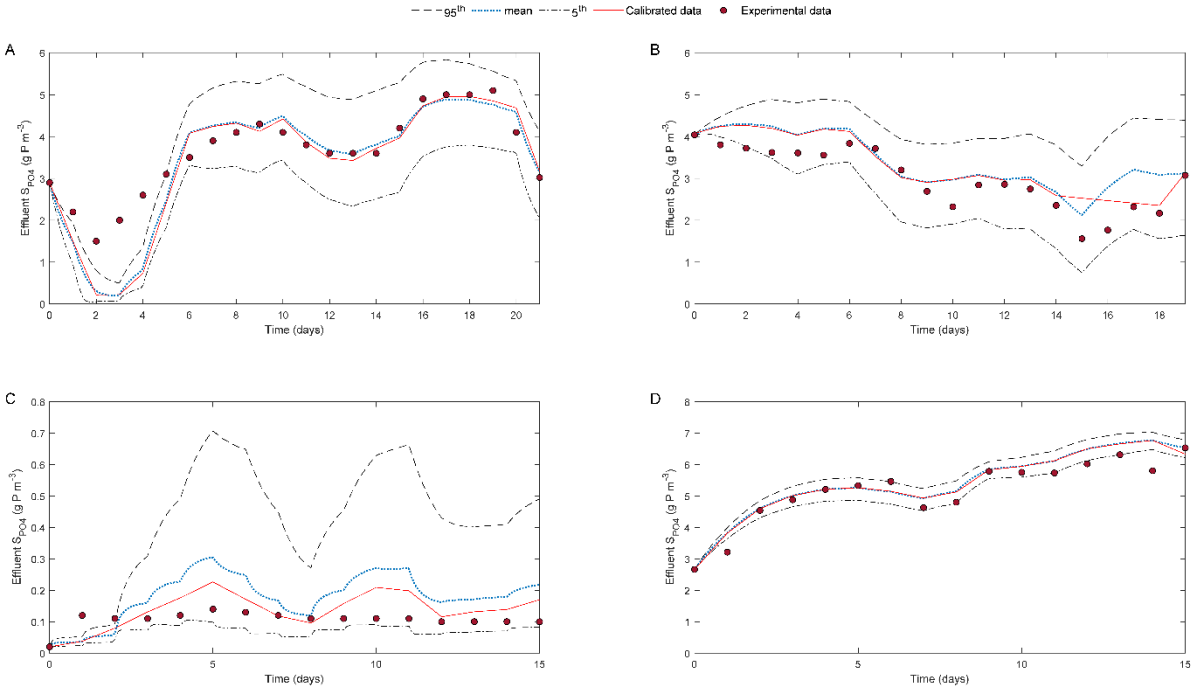

Figure 6

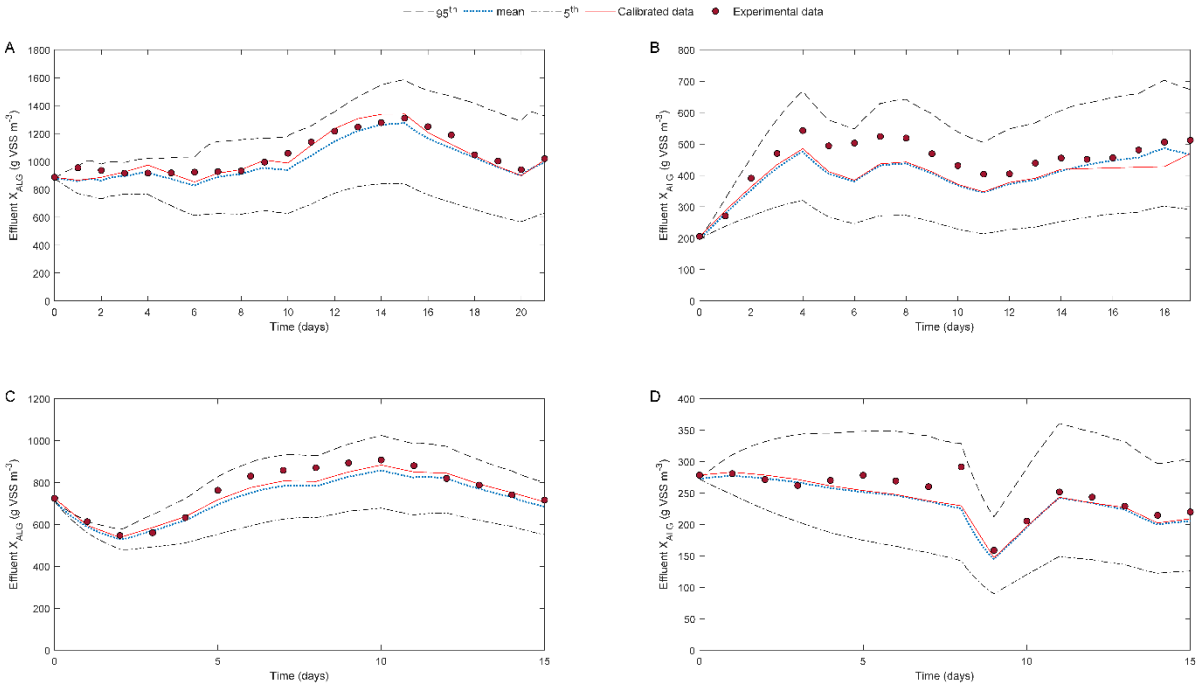

Figure 7

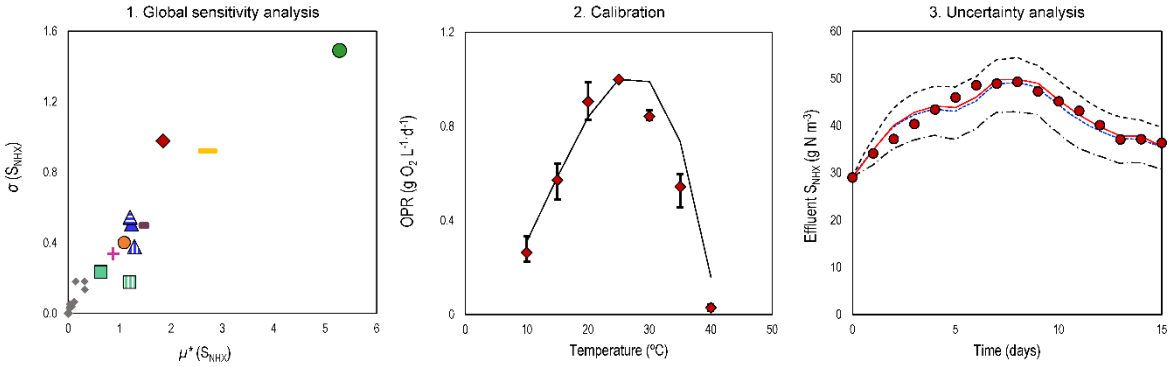

Graphical abstract